Pro Gradu:

Graphene Films for Gas Sensing Applications

Joni Hämäläinen
University of Jyväskylä
Department of Physics

As a part of Master of Science studies in Physics in University of Jyväskylä
June 2012 - May 2013
Advisors: Alexandre Satrapinski (MIKES), Antti Manninen (MIKES), Sergey Novikov (Aalto University)

Abstract:

Gas detection at small concentrations is usually done using transition metal oxides. These semiconductors are, however, strongly dependent on parameters and conditions of growth and processing. Graphene attracts a big interest in science and technology due to its exceptional electric properties, and this truly 2-dimensional material has a great promise to be used as highly sensitive gas sensor. In this thesis, CVD and epitaxial graphene samples have been investigated in order to improve their sensitivity in gas sensing applications. The response of the sensor to different concentrations of detected gas was observed as a relative change of resistance of the sample. The aim of this study was to find optimal parameters in application of a graphene based gas sensor, and to optimize the contacting area between graphene and metal for achieving stable contacts with low resistance. Three different kinds of metal-graphene contacts and several different metals for contacting to graphene were studied. Different temperatures and humidity levels as well as irradiation with 370 nm UV-light were used to find optimal conditions for sensing NO_2 gas. The sensitivity to O_3 was also studied. An optimized sensor exhibited response to 20 ppb concentration of O_3. In NO_2 detection, the response was increased significantly by heating samples above 100 °C. In a tested epitaxial SiC sample, the resistive response to 10 ppb concentration of NO_2 increased from 0.8 % in normal temperature to 1.4 % in elevated temperatures. Increasing of the temperature was also found to improve the linearity of response and to increase desorption rate of the molecules from graphene surface, allowing faster recovery after exposure. Annealed contacts with an additional graphite layer under the topmost metal layer, and with striped and dot-like geometry were found to have lower contact resistance (around 600 Ω) than a traditional contact with no additional patterning or graphite.

Tiivistelmä:

Pienten kaasupitoisuuksien mittaus on perinteisesti suoritettu erilaisilla metalli-oksidi-antureilla. Näiden puolijohdemateriaalien ominaisuudet ovat kuitenkin vahvasti riippuvia valmistusprosessin olosuhteista ja parametreistä. Grafeeni on tällä hetkellä tiedeyhteisön mielenkiinnon kohteena erikoisten sähköisten ominaisuuksiensa vuoksi. Tämä kaksiulotteinen materiaali tarjoaa mahdollisuuden erittäin pienien kaasupitoisuuksien tarkkaan mittaamiseen. Tässä työssä CVD- ja epitaksikasvatettuja grafeeninäytteitä on tutkittu niiden kaasuntunnistuskyvyn parantamiseksi. Myös kolmea erilaista metalli-grafeeni-kontaktia ja useita eri metalliyhdistelmiä tutkittiin. Tämän työn tavoitteena oli löytää parhaat mahdolliset ympäristöolosuhteet grafeeniantureiden resistiivisen vasteen mittaamiseen perustuvia kaasutunnistussovelluksia varten sekä pienentää kontaktiresistanssia ja parantaa metalli-grafeeni-kontaktien luotettavuutta. Optimaalisten olosuhteiden löytämiseksi grafeenin herkkyyttä NO_2-kaasulle testattiin eri lämpötiloissa, eri kosteusolosuhteissa ja 370 nm UV-säteilyn aikana. Grafeenin herkkyyttä O_3-kaasulle tutkittiin myös. 20 miljardisosan (ppb) O_3-pitoisuus riitti aiheuttamaan huomattavan muutoksen grafeenin resistanssissa. NO_2-mittauksissa resistiivistä vastetta eri kaasupitoisuuksille pystyttiin parantamaan huomattavasti lämmittämällä näytteitä yli 100 °C lämpötilaan. Resistanssin muutos huoneenlämmössä oli noin 0.8 % ja lämmityksen jälkeen noin 1.4 % epitaksikasvatetulle näytteelle 10 ppb:n NO_2-konsentraatiota mitattaessa. Korkeat lämpötilat myös paransivat vasteen lineaarisuutta ja nopeuttivat grafeenipinnalle adsorpoituneiden molekyylien desorptiota, puhdistaen grafeenin pintaa ja mahdollistaen nopean palautumisen altistuksesta kaasulle. Lämpökäsitellyt kontaktit ja grafiittikerros ylimmän metallikerroksen alla pienensivät kontaktiresistanssia. Pistemäisillä ja sormimaisilla kontaktityypeillä saatiin kontaktiresistanssia pienennettyä verrattuna perinteiseen suoraan kontaktipintaan. Sormimaisella, kahdesti lämpökäsitellyllä kontaktilla, jossa oli grafiittikerros ylimmän metallikerroksen alla, kontaktiresistanssi oli pienimmillään noin 600 Ω.

Acknowledgements

I would like to thank MIKES (Centre for Metrology and Accreditation) for the opportunity to work with an interesting new material, graphene, as well as for the inspiring and welcoming working environment. Special thanks to Alexandre Satrapinski and Antti Manninen for useful comments and discussions, and guiding me in my research, and to Sergey Novikov from Aalto University for all the help with this project. Thank you for all the patience and numerous corrections in writing of this thesis.

I would also like to thank Jari Walden from Finnish Meteorology Institute for the measurements done in FMI with precise equipment.

This work was supported in part via the joint research project Metrology for Chemical Pollutants in Air (MACPoll) of the European Metrology Research Programme (EMRP). The EMRP is jointly funded by the EMRP participating countries within EURAMET and the European Union.

Table of contents:

Table of used symbols:

Symbol	Units	Explanation
μ	cm^2/Vs	Mobility of the carriers
B	T	Magnetic flux density
C	part per million (ppm, 10^{-6}) part per billion (ppb, 10^{-9}) part per trillion (ppt, 10^{-12}) part per quadrillion (ppq, 10^{-15})	Concentration percentage of target gas in the carrier gas flow
e	C	Elementary charge, e=1.602·10^{-19} C
F	cm^3/min	Flow
I	A	Current
L, w, d	m	length, width and thickness of graphene
n	$1/cm^2$	Carrier concentration, number of carriers per square centimetre of graphene surface
q	C	Charge of the carriers
R	Ω	Resistance
R_0	Ω	Resistance of undisturbed device, initial resistance
R_{4T}	Ω	Resistance obtained by 4-terminal measurement
R_c	Ω	Resistance of a contact, contact resistance
R_{graph}	Ω	Resistance of graphene, excluding resistance of the contacts
R_{Tot}	Ω	Total resistance, Resistance of graphene including resistance of the contacts
R_{xy}	Ω	Resistance when measuring voltage perpendicular to current, Hall resistance

t	s	Time
U	V	Voltage
V	cm^3	Volume
ρ	$\Omega \cdot m$	Resistivity

1. Introduction

1.1. Gas sensors

Many toxic gasses are produced by factories and combustion engines, either as a side product of their main operation, or for use at some point of the process. Measuring and controlling the concentration of these gasses in the environment is a very important challenge for engineers and scientists today. Multinational organisations like EU or UN, as well as national regulations give strict limitations to pollution and require accurate measurement of small concentrations of toxic gasses.

Several different types of gas sensor devices already exist [1]. The gas whose concentration is to be measured, so called target gas, changes physical or chemical properties of these devices when it interacts with the active layer of a sensor. Comparing this change to a reference device without gas exposure, one can estimate the concentration of the target gas in the environment. A list of existing types of gas sensing devices and the physical quantities they use to detect gas is presented in Table 1. Some common types of gas sensor are described below.

In optical sensors an infrared light beam is partially absorbed by the target gas molecules. By detecting attenuation of the sensing beam the concentration of the target gas can be determined. Also different physical properties of the target gas, such as refractive index or fluorescence properties, can be used for measurements of concentration [1]. Optical gas sensors can be used in long distance detection. The light source and detection element can be placed a long distance from each other, and the average gas concentration on the path is sensed. Most other types of gas sensors are only capable of single point detection, at vicinity of the detecting element.

Other types of gas sensors include piezoelectric sensors, which use mass of the target gas to determine its concentration, and field effect sensors that measure the work function of target gasses to determine their concentration [1]. Catalytic gas sensors can sense combustible gasses by igniting them. Heat released in combustion is proportional to concentration of the target gas [2].

In semiconductor gas sensors, target gas molecules are adsorbed on the surface of semiconductor. They can either donate or accept electrons of the conduction band of the semiconductor, thus changing its conductivity. This conductance change can be detected with resistance measurement, and concentration of gas can be determined from the

magnitude of the change. These sensors are usually used at elevated temperatures, in order to improve their performance and reduce effects in the environment, such as humidity and temperature changes. Advantages of semiconductor sensors are their high sensitivity and small size [1]. On the other hand the response time and time of recovery from exposure are often long for semiconductor based gas sensors, and the relation between resistance change and concentration change is not linear [1]. Graphene sensors, which are the topic of this work, share many properties with semiconductor sensors.

Table 1 Types of solid state gas sensors and physical change they use for gas detection [1].

Type of devices	**Physical change**
Semiconductor gas sensors	Electrical conductivity
Field effect gas sensors: Diodes, transistors, capacitors	Work function (electrical polarization)
Piezoelectric sensors	Mass
Optical sensors	Optical parameters: SPR, reflection, interferometry, absorption, fluoresence, refractive index or optical path length
Catalytic gas sensors	Heat or temperature
Electrochemical gas sensors	Electromotive force or electrical current in solid state electrochemical cell

1.2. Graphene

Graphene is a monolayer sheet of carbon atoms in a honeycomb crystal lattice. Often a material consisting of few layers of these sheets is still called graphene [3]. This is why it is common to use such descriptions as monolayer, bilayer, few layer or multilayer graphene, according to the number of layers. This truly 2-dimensional material is a basic structural element for many other carbon allotropes, such as carbon nanotubes and graphite [3]. Graphene lattice is formed of carbon atoms bonded by a sp^2 bond [4]. Graphene was first obtained at Manchester University less than ten years ago, in 2004, by mechanical exfoliation

of graphite layers using adhesive tape [3]. Despite its short history, graphene has already been studied widely and it is a very promising material for semiconductor industry.

One of graphene's amazing properties is the zero band gap, which means that the conductivity of graphene can be altered by applying very little energy. However, for several applications non-zero band gap would be preferred, in order to "turn off" the device. Band gap opening on graphene has been proposed in several studies [3, 5].

Graphene is also known to have ballistic electron transport. It means that electrons moving on graphene surface have very long free paths, i.e. they can travel long distances without scattering [6]. This leads to a very low resistivity, another property that makes graphene attractive for industry and science. Quasiparticles in graphene have been found to act like relativistic Dirac fermions [7]. This means that in each corner of one Brillouin zone, electrons and holes seem to have zero effective mass. They act as if the speed of light was only 10^6 m/s, two orders of magnitude less that normal speed of light [3]. This is interesting for scientists studying relativistic effects. Usually it requires big and expensive machinery to reach relativistic speeds (i.e. accelerating particles near the speed of light), but with graphene, some relativistic phenomena can be studied in much slower velocities, meaning much less energy consumed and thus saving environmental and economical costs.

Three most common methods of graphene production are epitaxial growth from SiC, chemical vapour deposition on metal substrates (CVD), and mechanical exfoliation. Epitaxial growth and CVD, which have been used in this study, are described in more detail below. Mechanical exfoliation or micromechanical cleavage [3] was the first method used to produce graphene. It was initially a very crude method, but now it can be used to produce high-quality graphene up to 100 µm in size [3]. In this method graphene is derived from bulk graphite by peeling it using adhesive tape. Chemical exfoliation is another method, in which reactants are introduced to the graphite to reduce the van der Waals force between graphite layers [8]. Graphene can also be produced by reducing from graphite oxide, from aromatic molecules or benzene rings [8].

1.2.1. Epitaxial graphene

Epitaxial graphene is graphene grown on silicon carbide (SiC) surface. SiC wafers used for epitaxial growth of graphene are classified according to their unit cell structure. SiC is a compound made of stacked bilayers containing one layer of silicon atoms and one layer of carbon atoms. 4H-SiC is made of four of such bilayers in one unit cell [9]. Other types of SiC include 6H-SiC, which has six bilayers in a unit cell, and C-SiC, which has a cubic unit cell

structure [10]. When SiC wafer is heated above 1300 °C it starts to loose the top layers of Si, leaving one or few carbon layers on the top surface of the SiC substrate [11]. In this study 4H-SiC has been used for epitaxial growth at 1600 °C. Depending on parameters of the manufacturing process, one or more layers of graphene may be formed on the substrate. In this method of graphene growth the main problem is caused by defects of the wafer. When grown on SiC substrate, the crystal structure is copied layer by layer, so any defects on the bottom layer multiply when the number of layers is increased. These defects may include holes on graphene sheet, reaching either the SiC layer or the interface layer between graphene and SiC [10]. While an undoped SiC has no charge carriers at room temperature, the interface layer has some, but their mobility is strongly reduced in comparison to graphene [9,11]. The interface layer also affects physical properties of the graphene. It is proposed that the first layer of graphene grown on SiC is hole-doped due to the interface layer, and interaction between graphene and SiC may induce a gap opening between valence and conduction bands [10].

1.2.2. CVD

Chemical vapour deposition (CVD) is a method of growing graphene on a metal surface. The metal is heated and a gas containing carbon atoms is let to interact with the metal surface. During this process carbon atoms transfer from the source onto the metal surface and start forming honeycomb lattice [12]. This method is promising for manufacturing of graphene, but as the graphene is grown on a metal substrate, the graphene film must be removed and placed on another substrate in order to study its electrical properties. Using this method it is possible to manufacture big sheets of monolayer graphene. Fabrication of CVD graphene sheets with two or more layers is not yet possible, although a lot of study has been done in this area [13].

1.3. Graphene as a gas sensor

The graphene sheets have a large surface-to-volume ratio, which makes surface effects essential for the conductivity of the whole sheet. Gas molecules adsorbed on the top of the sensor change its conductivity by either donating or accepting electrons to/from the lattice and altering the charge carrier concentration in the lattice. Due to high electron mobility in graphene, even small changes in carrier concentration cause a big change in total resistance. That is a key feature for highly sensitive semiconductor gas sensors [14]. Graphene-based gas detectors are able to detect even a single molecule adsorbed on the surface [15].

A molecule of NO_2 gas is known to be an acceptor of electrons. Each NO_2 molecule changes the total charge of the carriers by about 0.1 *e* [16]. Whether this charge change

increases or decreases the resistivity of the sensor depends on the type of carriers in graphene. In pure, intrinsic graphene the Fermi level lies in the middle between conduction and valence bands, giving zero conductivity [17]. In practise, there are always some impurities present, and even a very small change in Fermi energy can increase carrier concentration and turn graphene into conductor. The point where conduction and valence bands get in touch is called the Dirac cone [18]. If the Fermi energy lies above this point, the graphene is n-type, and electrons are responsible for the conduction. If the Fermi energy lies below the Dirac point, the graphene is p-type [17,18]. The response of graphene to gas dependens on the initial position of the Fermi level. NO_2 exposure decreases carrier concentration of n-type graphene and increases carrier concentration of p-type graphene. The type of carriers in graphene may change during adsorption or desorption of some charged oxygen-including functional groups [19], or even NO_2 molecules [18]. This property can be used for gas sensing to differentiate the response between different gasses.

Graphene sensors have been shown to be able to detect e.g. NH_3 and CO_2 in ppm range [20,21]. The authors of Reference [22] report that sub-ppm level detection of NO_2 by graphene sensors has proved to be challenging, but they were able to detect 100 ppb of NO_2 in air (80 % N_2, 20 % O_2) using CVD graphene. Concentration of NO_2 even down to 40 parts per trillion (ppt) in pure N_2-gas has been sensed using graphene detectors by applying continuous in situ ultraviolet light illumination [23], and even individual NO_2 molecules have been detected in Reference [15]. Researchers of MIKES (Centre for Metrology and Accreditation) and Aalto University have recently reported that a relative resistance change of -45% in epitaxial graphene was obtained upon application of elevated temperatures and a gas mixture containing NO_2 at a concentration of 10 ppb [24]. By combining carbon nanotubes with reduced graphene the sensitivity and recovery time of graphene based gas sensors can be improved [25].

Ozone has been used to modify graphene sheets and to improve sensitivity of graphene to other gasses including NO_2 [26, 27, 28]. Ozone damages graphene surface by forming CO, CO_2, and epoxide groups on graphene [26, 27, 28]. No sensing experiments for ozone with CVD or epitaxial graphene have been reported before. Ozone concentrations below 100 ppb have been detected [29] with carbon nanotubes, which are graphene sheets rolled up into a tube.

No commercial gas sensors based on graphene exist yet, but a patent based on graphene sensor with in situ UV- irradiation has been issued by Honda Motor Co, Ltd [30]. The smallest concentrations detected by these devices were 40 ppt of NO_2, 10 ppt of NO, and 200

ppt of NH_3 [23, 30]. The sensors are theoretically capable of reaching detection limits of NO down to almost 150 parts-per-quadrillion (ppq), NO_2 to 2 ppt, and NH_3 to 33 ppt.

Measurements of the same type SiC samples and with the same measurement system as described in this study, have been done earlier by the researchers of MIKES and Aalto University as reported in [24]. In that article graphene samples epitaxially grown on SiC substrate exhibit response down to 10 ppb of NO_2 gas in air, but with longer times of exposure and recovery. Measurements results reported in [24] were performed only on NO_2 gas and only epitaxially grown graphene samples were used as sensors. In the present study both SiC and CVD graphene samples were investigated as sensors of NO_2 and also of O_3. Sensing of NO_2 was studied in low concentration range (10 ppb – 500 ppb), and measurement of ozone in high (up to 0.8 %) and low (20 ppb) concentrations.

1.4. Contact resistance

The density of electron states (DOS) is significantly higher in metal lattices than in semiconductors [31]. When carriers move from high DOS region into low DOS region, a potential barrier is formed between the two. This potential wall acts as an additional resistance, as electrons need to pass trough this potential [31]. In contacts between two metals, the DOS of both metals is nearly equal. Difference in work functions forces the electrons to redistribute at the contact, which creates an area of high resistivity. In normal metals, the length of this screening area is small so contact resistance is negligible [31]. In a contact between graphene and metal, DOS on both sides is similar, but the screening length is longer than that of metal-metal contacts. This is why metal contacts used to connect graphene have a high contact resistance [32]. Change of resistance in graphene when exposed to the measured gas is reduced or even hidden if the contact resistance between graphene and contacting metal electrode is too high.

To reduce the influence of this additional contact resistance, different methods can be used: 1) choose of suitable metals with low resistivity, 2) optimisation of the size and shape of contact pads, 3) increasing of the contact area. High work function of metals has been found to be beneficial in reducing contact resistance [31]. Bonding between metal and graphene also has influence on contact resistance. Contacts with strong chemical bonding have higher resistance but are more reliable during operation [32]. It has also been suggested that metal connected to graphene from the edge of the graphene lattice (end-contact) has significantly lower resistance and better mechanical stability than a metal contact at top of the graphene layer (side-contact) [33].

2. Experimental methods and set-ups

2.1. Sample configuration and contacts preparation

2.1.1. Lithography

Graphene films used in this study were fabricated by two methods: by sublimation of Si atoms in argon atmosphere at 1600 ºC from SiC wafer [24] and by CVD method (Single/Double Layer Graphene on 285 nm Silicon Dioxide Wafer, 10 Pack purchased from Graphene Supermarket). To configure the devices on a substrate, both epitaxial and CVD graphene samples were fabricated by the process described below (see Figure 1). Substrates with a graphene film were covered with AZ5214 resist, which was baked in 90 °C for twenty minutes. In the first step, the areas for metal contacts were exposed using Microtech 405 A laser writer on the resist. The resist on the area exposed with laser writer detaches from graphene surface when the resist is developed. The residual resist and graphene were removed from the contact areas by Ar/O_2-plasma. After this, the layers of metal were deposited by e-beam evaporation on top of the whole sample to form end-contacts with graphene. Layers of different metals can be deposited on the graphene sample, for example 5 nm of titanium covered by 50 nm of gold. Other used contact types were gold only and chrome and gold . Once the metal layer had been deposited, the sample was dipped in acetone. AZ5214 resist expands in acetone and removes the metal on top of it. The areas where there is no resist under metals are unaffected by the acetone treatment, and thus metals remain only in the places where resist was removed after development.

To make the graphene devices with Hall bar geometry and contacting area (presented in Figure 1), the samples were again covered by AZ5214 resist. Then the resist was removed from places where the graphene should not be present, and the graphene then was removed using Ar/O_2-plasma from areas not covered with resist. After the plasma treatment, the resist which was left on the graphene film was removed in acetone and the required configuration of the Hall bar device with the current and potential contacts was formed.

The final step of device lithography, in which the graphene-metal contact area was covered, was similar to the first contact deposition. Without the protective layer, contact interface could be easily destroyed by water molecules or ozone. Resist was applied over the whole sample, and removed from area around the graphene-metal interface. Materials used for covering the contacts were titanium (5 nm) and gold (50 nm). For some samples a layer of 5 nm of graphite was deposited before the Ti/Au layer, or 5 nm of chromium was used instead

of titanium. Metal outside the contact area was again removed by the acetone treatment. A photograph of the fabricated devices after lithography is presented in Figure 2.

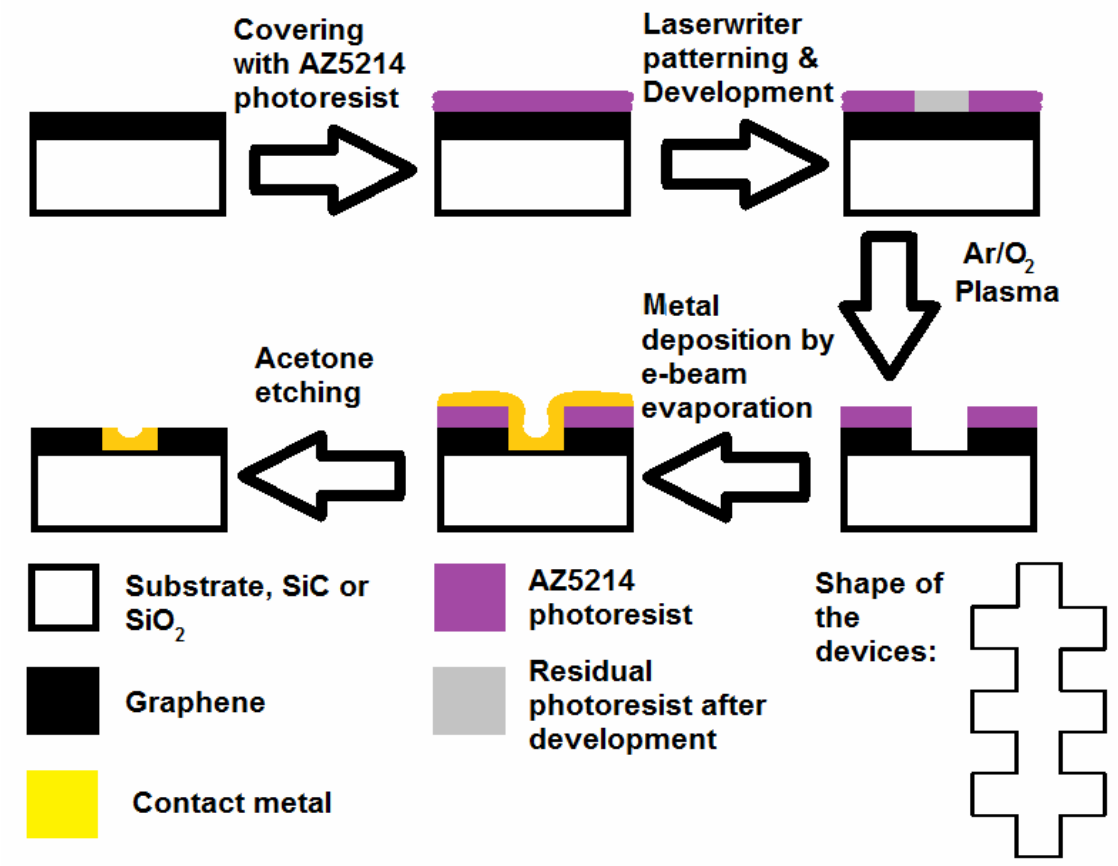

Figure 1. Description of the lithography process used for both epitaxial and CVD samples. The process consisted of three steps. First the metal contact pads are made. In the second step the Hall bars are shaped (no metal deposition is done in this step). In the third step the contacts are covered. Most commonly used contact metals were 5 nm of titanium covered with 50 nm of gold. Estimated thickness of the graphene was around 1-3 atomic layers, which means less than 1 nm. This is only a schematic figure, the thickness of graphene layer is much thinner compared to contact metal. The shape of the Hall bar devices is shown on lower right corner.

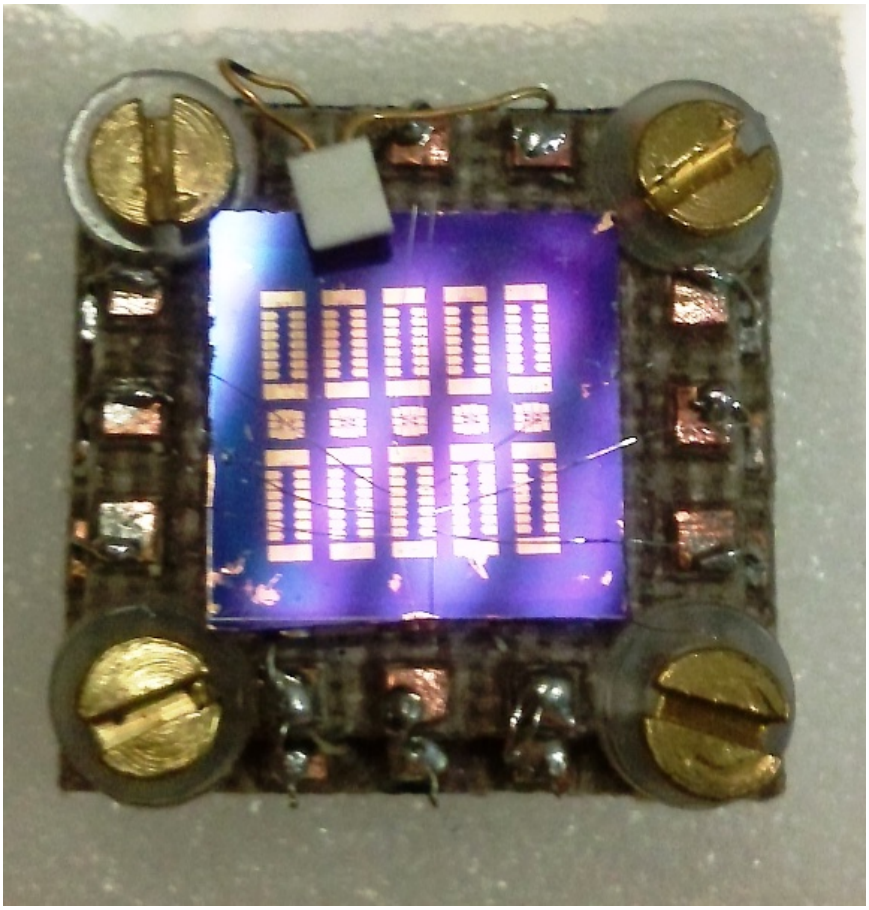

Figure 2. CVD120802 sample after lithography placed on a Teflon holder. This sample has 15 devices. The white probe on top of the sample is Pt100 resistor used as a temperature sensor.

2.1.2. Selection of devices

Each graphene chip had several Hall bar devices as shown in Figure 2. All contacts from all devices were measured under a microscope, and based on this measurement the device to be bonded was selected. Two needle probes were attached to pair of contacts, and voltage, *U*, was applied and swept from -1 V to 1 V. Resulting current, *I*, was measured using the same two probes. If the *I*-*U* curve showed a straight line, the contact was considered to be working and the resistance, *R*, was determined as [34]

$$R = \frac{U}{I}. \tag{1}$$

The smallest and equal resistance in all pairs of Hall bars was looked for.

2.1.3. Sample holders

After the preliminary measurement described above, the sample chips were attached to a holder with a double sided Scotch tape. Holders were made from copper covered Teflon plates in MIKES, using a PCB drill. Two Pt100 resistors were attached under the chip. One of them was used as a temperature sensor and one as a heater. Each holder had 12 pins. Four of the pins were reserved for Pt100 resistors, so eight of the pins were bonded to contacts on graphene devices. Bonding was done by ultrasound bonder in Micronova, Aalto University, using aluminium wire of diameter 25 µm.

2.2. Enclosure

For the gas measurement, a special enclosure for graphene samples was made. A photograph of the sensor and the brass enclosure is presented in Figure 3. All connections to the device go trough a hermetic 16 pin connector. The enclosure has two pipe connections for letting target gas in and out. The enclosure has a LED diode for UV-irradiation.

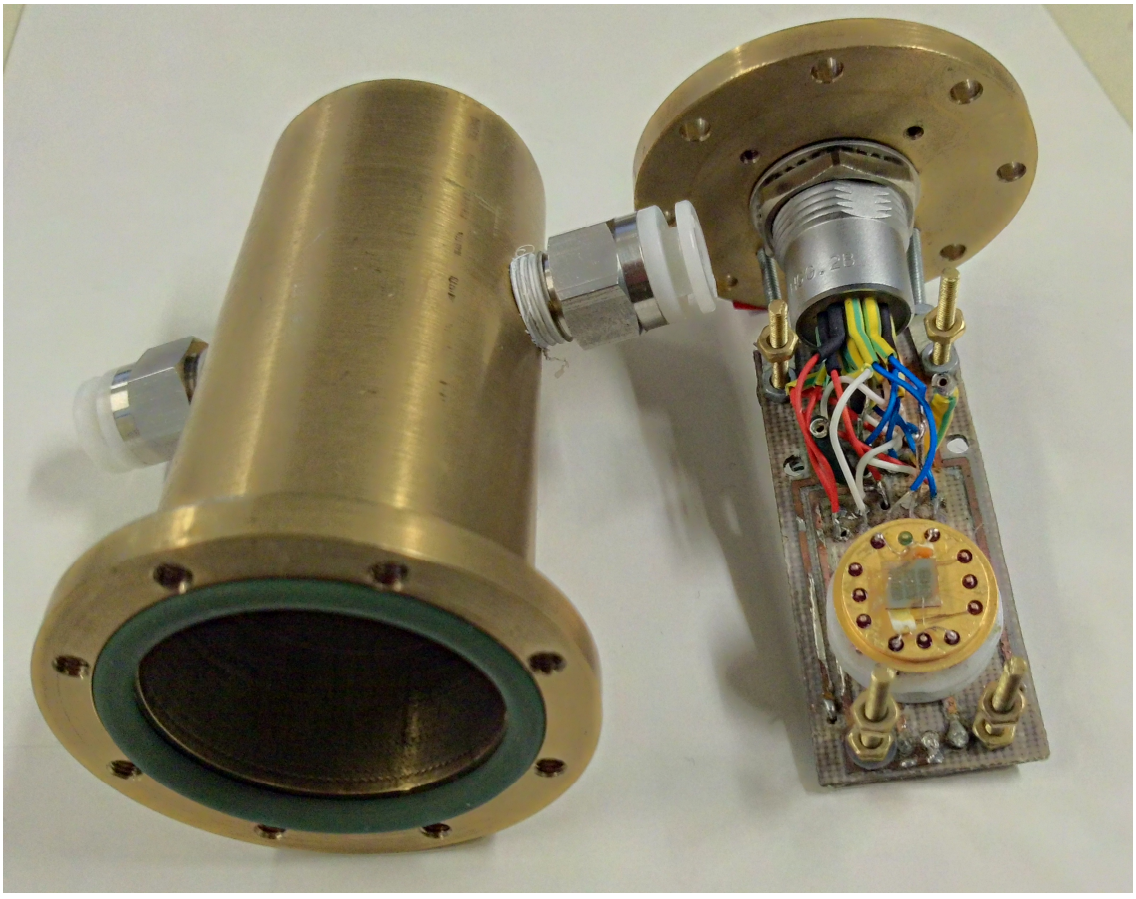

Figure 3. Enclosure for gas measurements and the sample holder.

2.3. Resistivity measurements

The resistivity of samples was measured by applying constant current trough current terminals (source and drain) in the ends of the channel of the device and measuring voltage from the potential contacts on the side of the channel (see Figure 4). In this way the effect of the contact resistances can be minimized. Knowing the dimensions of the device, the resistivity, ρ_{xx}, can be calculated as [34]

$$\rho_{xx} = R_{\mathrm{ab}} \frac{wd}{L_{\mathrm{ab}}} = \frac{U_{\mathrm{ab}}}{I_{\mathrm{sd}}} \frac{wd}{L_{\mathrm{ab}}}, \tag{2}$$

where U_{ab} and R_{ab} are the voltage and resistance between contacts *a* and *b* respectively, I_{sd} is the current applied from source to drain contact, *w* is the width, *d* is the thickness, and L_{ab} is the length of the channel from contact *a* to contact *b*. In reality the devices are not perfectly homogeneous so the voltages measured on different sides of the channel are not equal, but evaluating resistivity of graphene in this way is more accurate than two terminal measurements. Subscript *xx* in resistivity is used to indicate that voltage is measured in the same direction as current is applied; both in direction of *x* coordinate. In Hall measurement the voltage is measured perpendicular to the current, and the subscript is then *xy*.

Resistivity is directly related to two important material parameters that characterize graphene samples: number of charge carriers per square centimetre (carrier concentration) *n*, and their ability to travel in graphene, mobility μ. Electrical resistivity can be written in terms of *n* and μ as [34]

$$\rho_{xx} = \frac{d}{q\mu n}, \tag{3}$$

where *q* is the charge of the carriers. The carrier concentration here is the number of carriers per square centimetre. Often in literature, carrier concentration is given as carriers per cubic centimetre, but for graphene film which is essentially a 2-dimensional material, number of carriers per square centimetre is more generally used.

The quantity which is measured in this study is the resistance, *R*. Resistance can be directly calculated from the measured current and voltage, without knowledge of the dimensions of the sample, using Equation (1). To compare resistivity of samples of different sizes the results in this study are given as a relative deviation of resistance in % from the initial resistance.

For resistance measurements Keithley 236 source/meter unit was used. Keithley 236 has internal uncertainty of 0.1 % of the reading. Peak to peak noise of the samples resistance

measurement is around 0.1 %. Peak-peak noise is estimated from the measurements in MIKES with Agilent 3458A Digital Multimeter. Biggest uncertainty in resistance measurements comes from instability of environment (temperature, humidity, and pressure). The relative uncertainty of resistance due to environmental factors is evaluated to be around 1 %. These uncertainties can be combined as [35]

$$\delta Q = \sqrt{\sum_i (\delta q_i)^2} \tag{4}$$

where q_i are set of independent uncertainties and Q is their combined uncertainty. Using Equation (4) the relative uncertainty of resistance measurement is thus

$$\delta R = \sqrt{(1\%)^2 + (0.1\%)^2 + (0.1\%)^2} \approx 1\%.$$

When measuring relative change in resistance, both initial resistance R_0, and changing resistance R have uncertainty, so total relative uncertainty of deviation of resistance is about 1.4 %. This is only a preliminary estimation of uncertainty. Better estimation of uncertainties would require additional measurement and analysis.

2.4. Contact resistance measurements

To evaluate contact resistance, contacts are considered as two extra resistors in series with the resistance of graphene film sample. Resistivity of graphene can be measured with four terminal measurements of the sample having Hall bar geometry (see Figure 4). Contact resistance can be calculated from resistivity and two terminal measurements of the total resistance of the film and the contacts. The scheme of device and dimensions used in measurements are presented in Figure 4. The two terminal resistance of the total length $R_{\mathrm{tot,2T}}$, including the resistance of the contacts, can be expressed as

$$\frac{U_{\mathrm{2T}}}{I_{\mathrm{sd}}} = R_{\mathrm{tot,2T}} = 2R_{\mathrm{c}} + R_{\mathrm{graph}}\,, \tag{5}$$

where U_{2T} is the voltage between the current contacts, R_{graph} is the resistance of the graphene film, not including the resistance of the contact area, and R_c is the resistance of one contact.

From the measurement of voltage between two potential contacts, $U_{\mathrm{mid,4T}}$, the four terminal resistance, $R_{\mathrm{mid,4T}}$, can be calculated using Equation (1). The resistivity, ρ_{xx} is obtained from Equation (2) knowing the distance between two potential contacts L_{ab}, the width of the graphene film w, and the thickness of the graphene d. From ρ_{xx}, the resistance R_{graph} between the end contacts with distance L_{graph}, can be calculated. The contact resistance then is calculated from $R_{\mathrm{tot,2T}}$ and $R_{\mathrm{mid,4T}}$ as

$$R_{\mathrm{tot,2T}} = 2R_{\mathrm{c}} + R_{\mathrm{graph}} = 2R_{\mathrm{c}} + \rho_{xx}\frac{L_{\mathrm{graph}}}{wd} = 2R_{\mathrm{c}} + R_{\mathrm{mid,4T}}\frac{wd}{L_{\mathrm{ab}}}\frac{L_{\mathrm{graph}}}{wd}$$
$$\Leftrightarrow R_{\mathrm{c}} = \frac{1}{2}\left(R_{\mathrm{tot,2T}} - R_{\mathrm{mid,4T}}\frac{L_{\mathrm{graph}}}{L_{\mathrm{ab}}}\right). \quad (6)$$

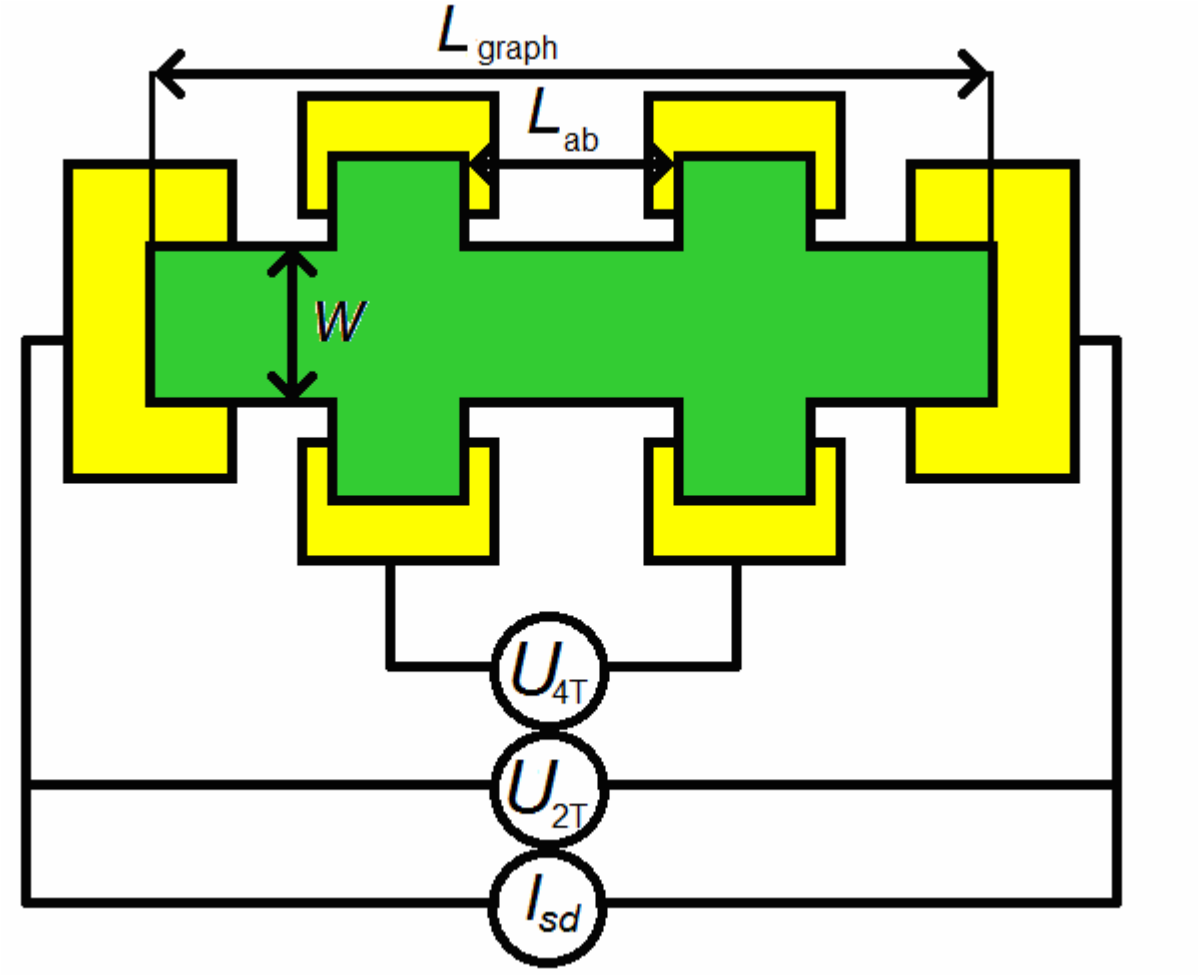

Figure 4. Scheme of measurement terminals and dimensions used for estimation of contact resistance. The resistance of the whole graphene film can be evaluated by measuring the resistance between two potential contacts and using that to calculate the resistance of whole graphene film. Difference between two terminal resistance (U_{2T}/I_{sd}) and the calculated graphene resistance is due to the contact resistance between graphene and metal in the current contacts.

2.5. Measurement of mobility and carrier concentration

Mobility and carrier concentration of the graphene films were determined using Hall effect [36]. When a conductor carrying a current is in magnetic field perpendicular to the current, the magnetic force turns the charge carries towards one side of the conductor, and a potential difference proportional to magnetic field is created between the sides of conductor perpendicular to the current [36]. This voltage can be used to evaluate transverse, or Hall resistance, R_{xy}. The change in R_{xy} when magnetic flux density B is changed, depends on carrier concentration and charge of the carriers [34]

$$\frac{dR_{xy}}{dB} = \frac{1}{qn}. \tag{7}$$

This equation is used for estimation of carrier concentration n. Mobility μ was evaluated from n and Equation (3).

2.6. Gas sources for ozone and NO_2 experiments

In preliminary measurement of the graphene response to O_3, the Fischer 500M generator was used as an ozone source. Using a similar device [37] maximum ozone concentration has been estimated to be 7800 ppm. This is the maximum concentration of O_3 created from air flow. Ozone generator has a control of output of O_3 that ranges from 1 % to 100 % of the maximum concentration (7800 ppm). This approximation for concentration of O_3 is rather rough and has estimated relative uncertainty of about 10 % which is enough for the present measurement but can be re-estimated if more accurate measurements are needed. Ozone measurement was performed in stainless steel enclosure, similar to the brass enclosure (Figure 3).

NO_2 measurements were done in Micronova, Aalto University. The gas system is presented in Figure 5. Dry air which flows into the enclosure is controlled by a mass flow controller. For operation at low humidity, some of the dry air was directed trough water. For the high humidity range, the whole air flow was directed trough water. Originally prepared gas with 10 ppm concentration of NO_2 was diluted with artificial air (20 % O_2 and 80 % N_2). The flow of diluted NO_2 was also controlled by mass flow controller. Normal flow of dry air was 1000 cm^3/min, humid air flow in low humidity measurement 100 cm^3/min, and maximum flow for NO_2 was 100 cm^3/min. Concentration of NO_2 , C_{NO2}, in the air flow was estimated as

$$C_{\mathrm{NO2}} = \frac{F_{\mathrm{NO2}}}{F_{\mathrm{tot}}} \cdot 10\,\mathrm{ppm} = \frac{F_{\mathrm{NO2}}}{F_{\mathrm{air}} + F_{\mathrm{humid}} + F_{\mathrm{NO2}}} \cdot 10\,\mathrm{ppm} = \frac{F_{\mathrm{NO2}}}{1100\,\frac{\mathrm{cm}^3}{\mathrm{min}} + F_{\mathrm{NO2}}} \cdot 10\,\mathrm{ppm}\,. \qquad (8)$$

Here F_{NO2} is the flow of diluted NO_2 gas, F_{tot} is the total flow going into the measurement enclosure, F_{air} is the flow of dry air, and F_{humid} is the flow of humid air.

For example minimum flow of 1 cm^3/min of diluted NO_2 gives concentration

$$C_{\mathrm{NO_2}} = \frac{F_{\mathrm{NO2}}}{F_{\mathrm{tot}}} = \frac{1\,\frac{\mathrm{cm}^3}{\mathrm{min}}}{1100\,\frac{\mathrm{cm}^3}{\mathrm{min}} + 1\,\frac{\mathrm{cm}^3}{\mathrm{min}}} \cdot 10\,\mathrm{ppm} \approx 0.009\,\mathrm{ppm} = 9\,\mathrm{ppb}\,.$$

During measurements it was noticed that the used brass enclosure adsorbs some amount of NO_2, which increases uncertainty for the actual concentration sensed by the graphene devices. The test measurements performed in Finnish Meteorological Institute showed that about 10 % of input concentration of NO_2 was lost in the enclosure.

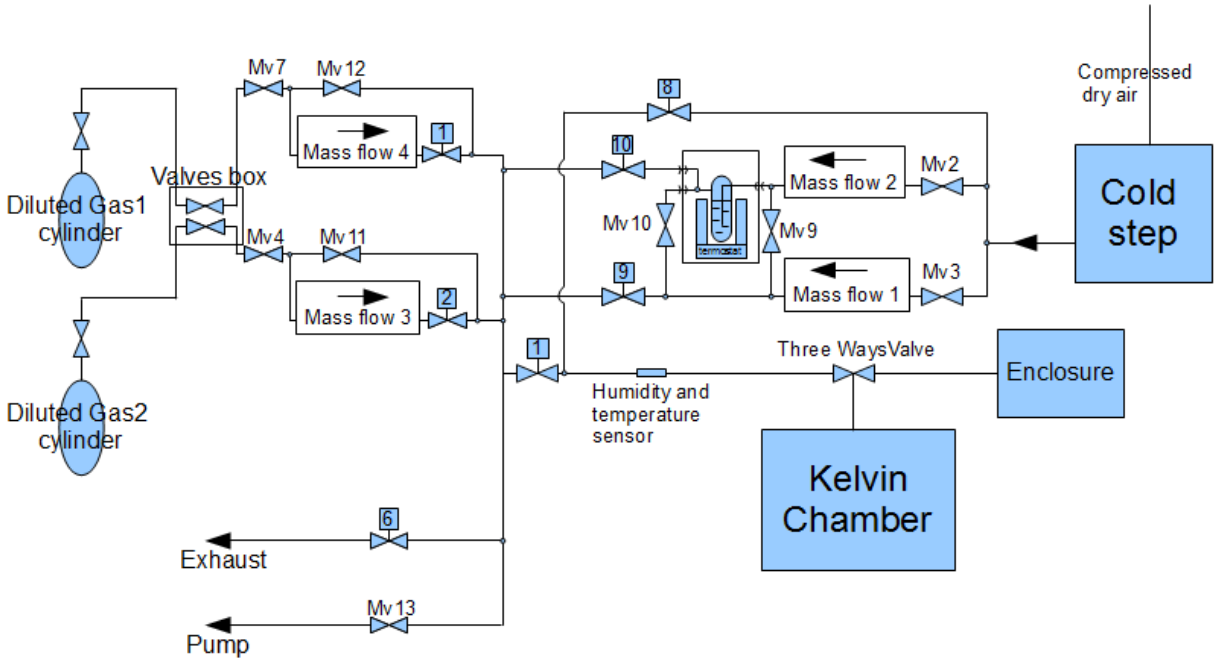

Figure 5. Gas system in Aalto University. Three mass flow controllers control the flow of dry air (Mass flow 1), humid air (Mass flow 2), and NO_2 (Mass flow 3). Gas system could be modified to use two different target gasses, but in this study only NO_2 was used (Gas2).

2.6.1. Estimation of uncertainty of NO_2 gas concentration.

The main sources of uncertainty of the actual concentration of NO_2 gas supplied for the measurements comes from four main parts: 1) uncertainty of the original concentration of NO_2 gas (10 ppm), depending on the specification of manufacturer, 2) uncertainty of the dilution of the reference gas from original 10 ppm to desired concentration, 3) use of the materials in supporting elements, changing an applied gas concentration, and 4) presence of residual gasses and random fluctuations in flow around the graphene sensor.

The manufacturer of the diluted gas states that the purity of NO_2 gas is within 1 % of the actual amount of pure NO_2, and the uncertainty of the dilution concentration is 2 % of the original announced 10 ppm.

Aera FC-D980 Mass Flow Controller used to vary concentration of NO_2 has specified internal uncertainty of ±0.25 % of the value, when the gas flow is under 25 cm^3/min (concentration < 250 ppm), and ±1 % when the flow is higher. Dry air flow has variation within ±1 %.

Influence of the used material in supporting parts of the sensor enclosure was tested in the Laboratory of Air Quality, in Finnish Meteorological Institute (FMI). The enclosure for

holding the sensor is made of brass and in the measurements performed in FMI with a calibrated NO_2 source and detector, the NO_2 concentration of output gas was about 10 % less than the concentration of the input gas. Teflon holder for the graphene chips is inert and should not influence the gas concentration around the graphene surface.

Presence of residual gasses and random fluctuations in the flow around the graphene sample are estimated to have an relative uncertainty of about 1.5 %.

Combining these four components using Equation (4) we can approximately estimate that the total relative uncertainty of NO_2 concentration of the supplied gas is around 10 %, which is enough for the present investigation of the sensing abilities of graphene sensors.

2.7. Equipment for UV-irradiation and heating

Influence of UV-irradiation and temperature on resistivity of graphene and its response to NO_2 gas was studied. UV-irradiation was obtained from 370 nm UV-LED diode with optical power of 1 mW. UV-LED diode was located about 1 cm away from the surface of graphene. To heat the samples up to 150 °C, a Pt100 resistor placed under the chip with graphene was used. Another Pt100 resistor was used to measure the temperature. To study the influence of UV irradiation and temperature on carrier concentration and mobility of graphene films, the Hall measurements in low field were done before and after UV-irradiation, and during heating.

3. Experimental results

3.1. Temperature dependence

To estimate temperature dependence of graphene's resistivity, samples were heated from 22 °C up to 40 °C. Results from these measurements are presented in Table 2. Resistances of different samples have very different temperature coefficients, from about - 1.6 % / °C to about + 1.3 % / °C. Most of the samples showed decrease of resistance with increase of temperature. One reason for different responses to temperature change can be the residual gasses and impurities that are desorbed from graphene when it is heated. The residual gasses may include electron acceptors (such as NO_2 , O_3) or electron donors (such as NH_3, CO, NO) [16]. Also the carrier type of the graphene sample can be either n- or p- type, so desorption of the same gas from the different graphene surfaces can cause different changes in resistance. Without the effect of desorption, resistance of pure semiconductors should decrease due to thermal excitation of carriers when heated [34]. Resistance of metals should increase because

of increase in scattering from phonons and other electrons [34]. Graphene may exhibit both semiconductor-like and metallic (or semi-metallic) behaviour, depending on the method of manufacturing, quality of the sample, and interaction with the substrate [11,12,18].

Table 2. Temperature coefficients of the resistance of the tested graphene samples measured in temperature range of 20 °C - 40 °C. Measurements were performed in open enclosure. Pt100 resistor was used as a heater with 1 W of maximum applied power. Temperature was measured by another Pt100 resistor placed close to the graphene film. The results are given as ratio of relative change of resistance (in %) and change of temperature.

Sample	Tc (% / °C)
CVD120718#2	-0.1
CVD120802Ti	+1.3
CVD120802Au	-0.7
CVD120912Ti	-1.6
CVD120912Cr	+0.3
SiC120903	<+0.06

3.2. UV-irradiation

The tested graphene samples were irradiated by UV-LED with 370 nm emission wavelength for 30 minutes. The results of resistance measurement during irradiation are presented in Figure 6. All samples showed increase of resistance while being irradiated. The increase of resistance in CVD samples was between 60 % and 110 %. SiC samples were less sensitive to UV: their resistance changed by 8 % - 15 %. The resistance of SiC120516 sample decreased immediately when the UV-light was turned on, and increased rapidly when UV-light was turned off. This phenomenon did not appear in tested CVD samples. The measured temperature change of graphene during UV-irradiation was less than 1 °C, which did not affect the observed variations in resistance. Changes in resistance reflect mostly the reduction of charge carriers concentration and possibly their mobility and the quantitative estimation of these effects is given in the next section.

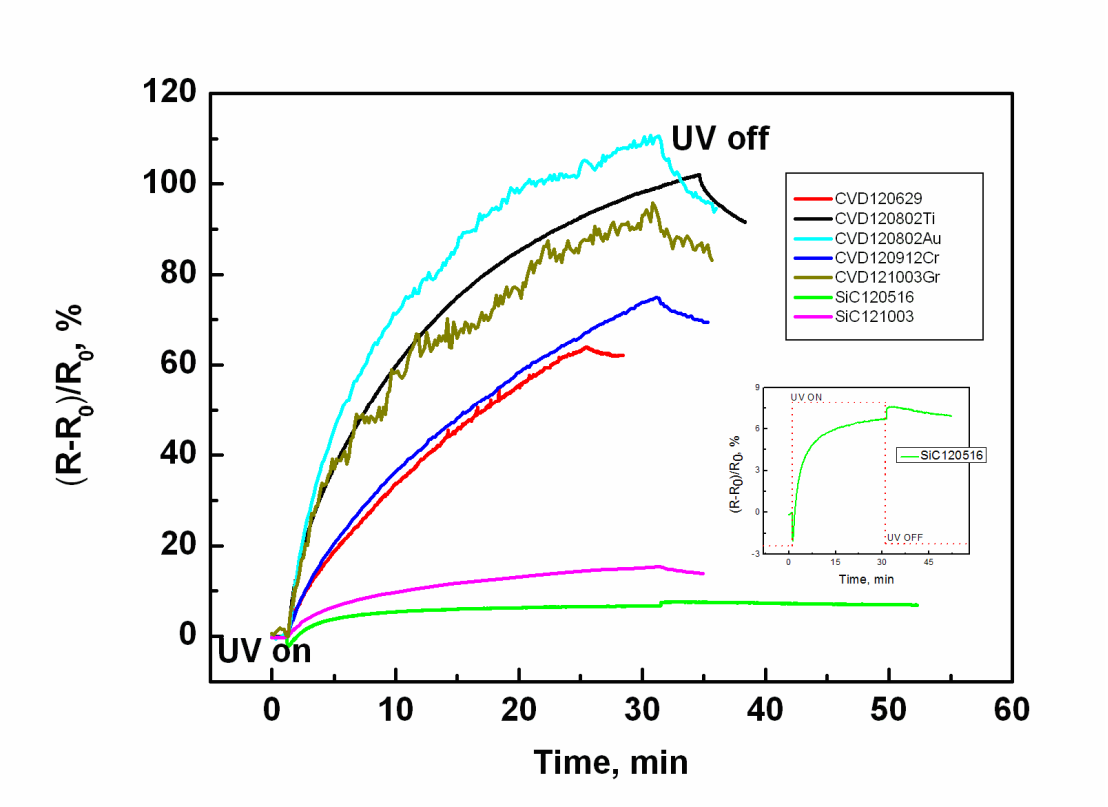

Figure 6. Effect of UV-irradiation. The effect is much larger in tested CVD samples than in SiC samples. Recovery from the exposure to UV-irradiation is slow and can take several hours until resistance returns to original value. A small instant drop in resistance is noticed in SiC samples, and resistance increases again when UV-light is turned off. Similar effect does not appear in tested CVD samples. The inset shows response of SiC120516 in detail.

3.3. Influence of UV-irradiation and heating on mobility and carrier concentration

To evaluate the effects of UV-irradiation and temperature on carrier concentration and mobility, a measurement of the Hall resistance, R_{xy}, was done before and after heating and UV-irradiation. Carrier concentration was calculated as:

$$n = \frac{1}{q\dfrac{dR_{xy}}{dB}} \tag{9}$$

(see Equation (7)). By measuring longitudinal resistance, the resistivity of graphene film was estimated using Equation (2), and the mobility was calculated combining Equations (2), (3) and (7):

$$\mu = \frac{d}{\rho_{xx} q n} = \frac{I_{sd}}{U_{ab}} \frac{L_{ab}}{w} \frac{dR_{xy}}{dB}. \tag{10}$$

An example of the results of measurement of the Hall resistance of one CVD graphene sample is presented in Figure 7. The CVD120912Ti sample's Hall resistance changed by 7 Ω when this sample was inserted into a magnetic field of 0.1 T. From Equation (9) the carrier concentration was calculated as

$$n = \frac{1}{1.6*10^{-19}\ \mathrm{C}\cdot\frac{7\,\Omega}{0.1\,\mathrm{T}}} = \frac{1}{1.6*10^{-19}\,\mathrm{As}\cdot\frac{7\,\Omega}{0.1\cdot10^{-4}\ \mathrm{Vs/cm^2}}} = 9\cdot10^{12}\,\frac{1}{\mathrm{cm^2}}.$$

The measured resistivity of CVD120912Ti was 1.7 μΩm, so the carriers mobility was calculated using Equation (10)

$$\mu = \frac{10^{-9}\ \mathrm{m}}{1.7\cdot10^{-6}\ \Omega\mathrm{m}\cdot1.6\cdot10^{-19}\ \mathrm{C}\cdot9\cdot10^{12}\,\frac{1}{\mathrm{cm^2}}} = 400\frac{\mathrm{cm^2}}{\mathrm{Vs}}.$$

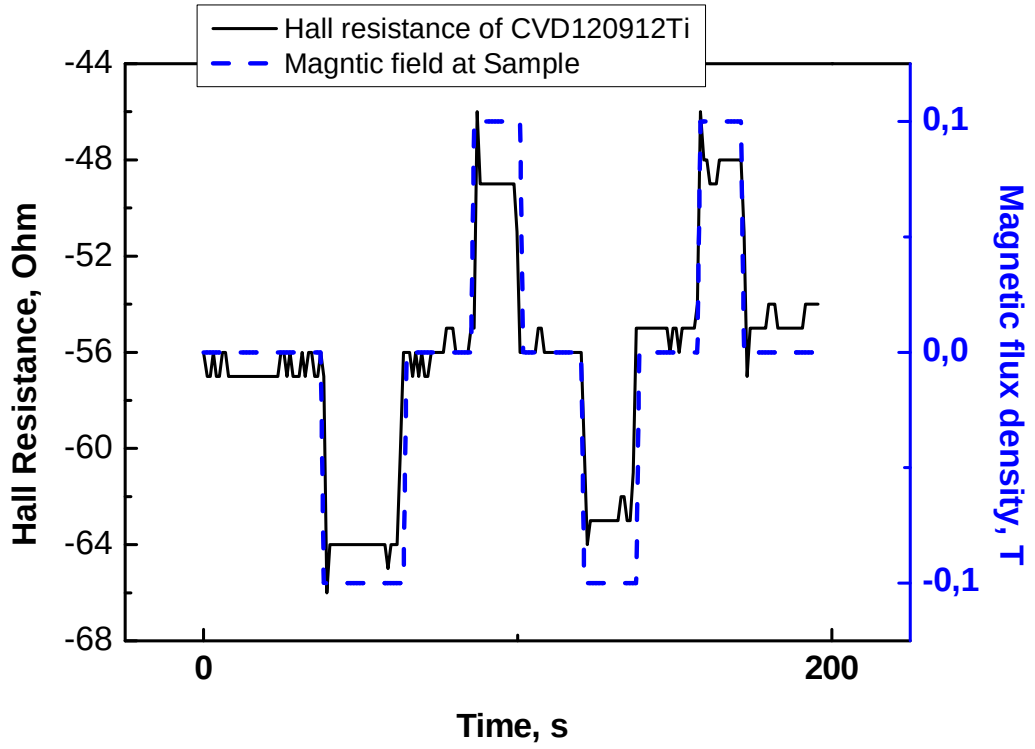

Figure 7. Hall resistance measurement on CVD120912Ti sample in magnetic fields between -0.1 T and +0.1 T.

Results of the influence of heating on the mobility and carrier concentration of three CVD samples are presented in Figure 8. The samples were heated up to 50 °C using a Pt100 resistor placed underneath of the holder, with about 1 W heating power. Mobility increases in all three samples, most of all in CVD121009Eu, the sample which is covered by europium. With increasing temperature, the mobility of graphene samples CVD121009Eu,

CVD120718#1, and CVD120802Ti, increases from 2000 cm^2/Vs to 4500 cm^2/Vs, from 5000 cm^2/Vs to 6000 cm^2/Vs, and from about 290cm^2/Vs to 430 cm^2/Vs, accordingly. Carrier concentrations in all tested samples decreased. Carrier concentration of CVD121009Eu, CVD120718#1 and CVD120802Ti decreased from $12 \cdot 10^{11}$ /cm^2 to $5 \cdot 10^{11}$ /cm^2, from $14 \cdot 10^{11}$ /cm^2 to $13 \cdot 10^{11}$ /cm^2, and from about $4.7 \cdot 10^{11}$ /cm^2 to $3.3 \cdot 10^{11}$ /cm^2, accordingly. Overall resistance decreased in all samples during heating from 14 kΩ to 12 kΩ in CVD121009Eu, from 4.4 kΩ to 4.0 kΩ in CVD120718#1, and from 15 kΩ to 14 kΩ in CVD120802Ti.

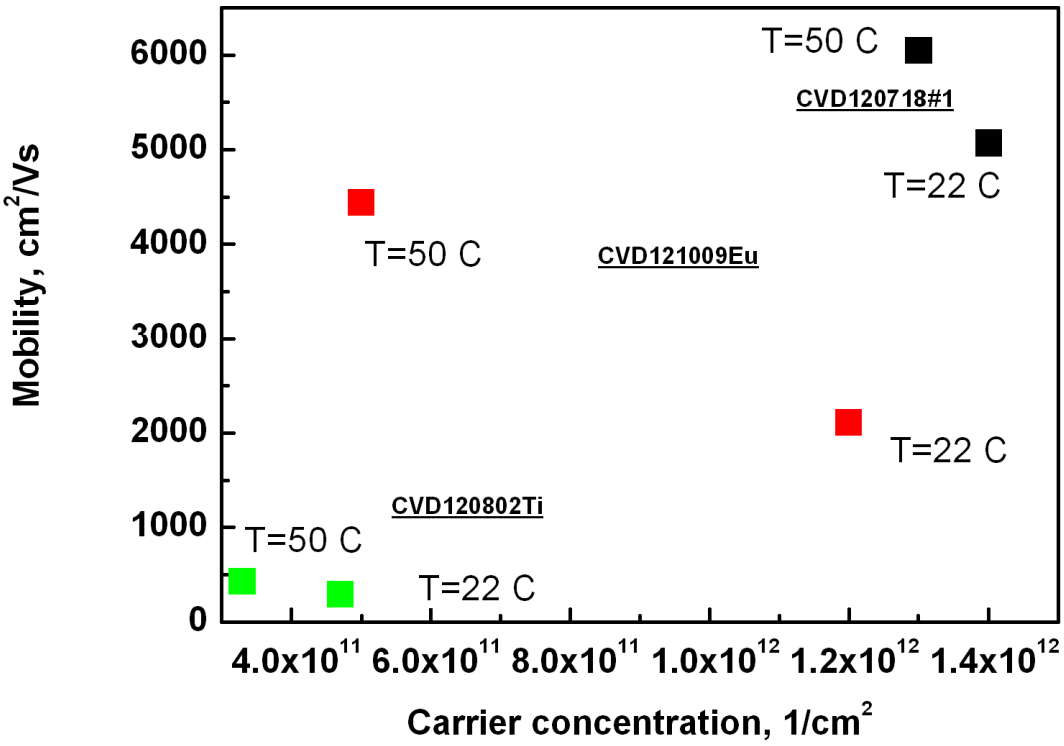

Figure 8. Effect of heating on carrier concentration and mobility of the charge carriers in tested CVD graphene samples. Mobility of samples increases while carrier concentration decreases. The resistance decreases during heating for all tested samples.

The results of the influence of UV-irradiation on the Hall resistance measurement performed before and immediately after irradiation, which had lasted for 8 minutes, are presented in Figure 9. The samples were irradiated with UV-LED diode located about 1 cm away from the surface of graphene. The temperature of the devices increased slightly during the measurement, but less than 1 °C.

The mobility increased in all samples. In CVD121009Eu, CVD120718#1, and CVD120802Ti, mobility increased from 3000 cm^2/Vs to 4000 cm^2/Vs, from 5500 cm^2/Vs to

6500 cm^2/Vs, and from 300 cm^2/Vs to 320 cm^2/Vs. Carrier concentration in all tested samples decreased. In CVD121009Eu, CVD120718#1, and CVD120802Ti, concentration decreased from $11 \cdot 10^{11}$ /cm^2 to $6 \cdot 10^{11}$ /cm^2, from $16 \cdot 10^{11}$ /cm^2 to $11 \cdot 10^{11}$ /cm^2, and from $6 \cdot 10^{11}$ /cm^2 to $5 \cdot 10^{11}$ /cm^2. Overall resistance increased in all samples during UV-irradiation from 9 kΩ to 14 kΩ in CVD121009Eu, from 3.6 kΩ to 4.5 kΩ in CVD120718#1, and from 13 kΩ to 15 kΩ in CVD120802Ti. Thus UV-irradiation and heating have similar effects on the mobility and carrier concentration of graphene, but they have opposite effect on resistance.

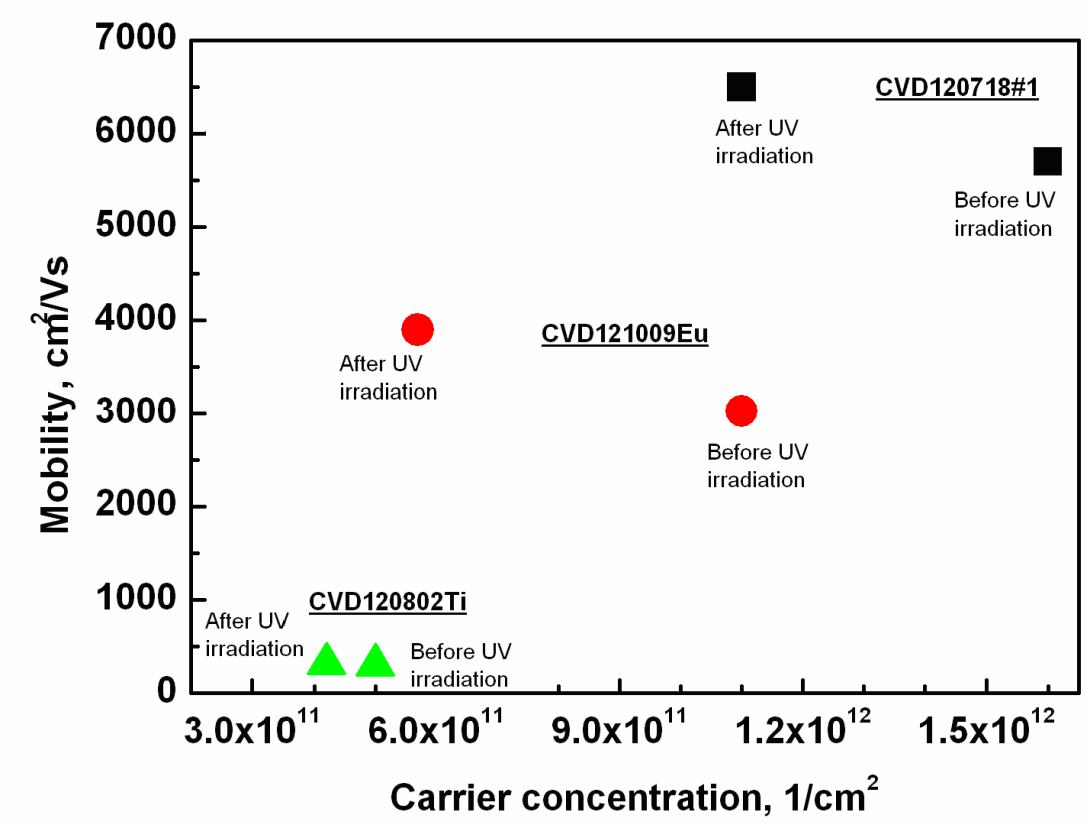

Figure 9. Carrier concentration and mobility before and after UV-irradiation. Samples were irradiated during 8 minutes with 370 nm wavelength UV-light with optical power of 0.75 mW. UV-LED diode was located about 1 cm away from the graphene surface. Carrier concentration decreases and mobility increases when UV-irradiation is applied, but the resistance of the devices increases during UV-irradiation.

Higher mobility after UV-irradiation may be due to heat. Increase of carrier concentration can be explained by increase of doping due to UV-light [38]. UV-light may produce some ozone. Ozone is an electron acceptor and decrease of carrier concentration should indicate graphene to be of n-type. Ozone exposure may also cause defects to form on graphene surface as ozone and carbon form epoxide groups [39]. Effects of ozone creation should however be suppressed

because the wavelength of the UV-light was at the high end of UV-spectrum, 370 nm. That is not normally energetic enough to create ozone from atmospheric oxygen [40]. If UV-irradiation changes electronic properties of graphene, not just by creating impurities or by heating, it can be used to increase sensitivity of graphene based gas sensors.

3.4. Improvements in graphene-metal contacts

Contact resistance was studied for SiC graphene samples with different structures, configurations and shapes of the contact pads [41], which are presented in Figure 10. All graphene samples used in this study, their parameters and used materials of the first and second metallization are presented in Table 3. The contact configuration was optimized in order to reduce the contact resistance. In [33] the contact resistance for different geometries was calculated and it was shown that for all metals in the “end-contacted” configuration (where the contact between metal and graphene is formed on the “ends” of graphene) the contact resistance is significantly less, compared to “side-contacted” configuration (where the contact between metal and graphene is formed along the graphene plane and metal is on top of the graphene film). In order to increase the end-contacted fraction of contact between metal and graphene, the contact area was patterned using stripe (A) and dot-like (B) shapes as shown in A and B panels of Fig 10. For comparison the contacting area in devices in panel C had no additional patterning.

Our improved layout has several advantages: 1) contact pads deposited directly to SiC surface without graphene have much better adhesion, 2) short metal bridges between stripes and dots is less inclined to exfoliation, 3) stripe and dot-like array shapes have more fraction of end-type of contact compared to the conventional geometry, 4) bonding wires are attached to the contact pads, to the first metallization layer, and do not damage the graphene film.

Table 3. Tested graphene samples, their parameters and materials of the first and second metallization.

Sample name	Growth method	Substrate	Contact type metal-graphene-metal		No. of devices on chip	Covered
			First metallization	Second metallization		
CVD120629	CVD	SiO_2	Ti/Au	Ti/Au	45	No
CVD120718#1	CVD	SiO_2	Ti/Au	Ti/Au	45	No
CVD120718#2	CVD	SiO_2	Ti/Au	Ti/Au	45	PMMA
CVD120802Ti	CVD	SiO_2	Ti/Au	Ti/Au	15	PMMA
CVD120802Au	CVD	SiO_2	Au	Au	15	No
CVD120912Ti	CVD	SiO_2	Ti/Au	Ti/Au	15	No
CVD120912Cr	CVD	SiO_2	Cr/Au	Cr/Au	15	No
CVD121003Gr	CVD	SiO_2	Ti/Au	C/Ti/Au	15	No
CVD121009Eu	CVD	SiO_2	Ti/Au	Ti/Au	15	Europium
SiC1312	Epitaxial	SiC	Ti/Au	Ti/Au	7	Europium
SiC120516	Epitaxial	SiC	Ti/Au	Ti/Au	7	No
SiC120903	Epitaxial	SiC	Ti/Au	Ti/Au	3	No
SiC121003	Epitaxial	SiC	Ti/Au	Ti/Au	3	Europium
SiC121030	Epitaxial	SiC	Ti/Au	Ti/Au	6	No
SiC121101	Epitaxial	SiC	Ti/Au	C/Ti/Au	6	No
SiC121012	Epitaxial	SiC	Ti/Au	Ti/Au	6	No
SiC121010	Epitaxial	SiC	Ti/Au	Ti/Au	6	No

In total four different samples with this mask were produced. For all of these samples (SiC121030, SiC121101, SiC121012 and SiC121010) first metallization was done with 5 nm of titanium and 50 nm of gold. In SiC121030, contacts were covered with 5 nm of titanium and 50 nm of gold during the second metallization. Contacts of SiC121030 were not annealed. SiC121012 and SiC121010 contacts were annealed, and covered with titanium/gold. In SiC121101 contacts were covered during the second metallization with a 5 nm layer of graphite followed by the deposition of the titanium/gold. Annealing was done twice for

SiC121101. Lithography process is presented in Figure 1. The resistance of each device was measured by two terminal and four terminal methods, and contact resistances were calculated using Equation (6).

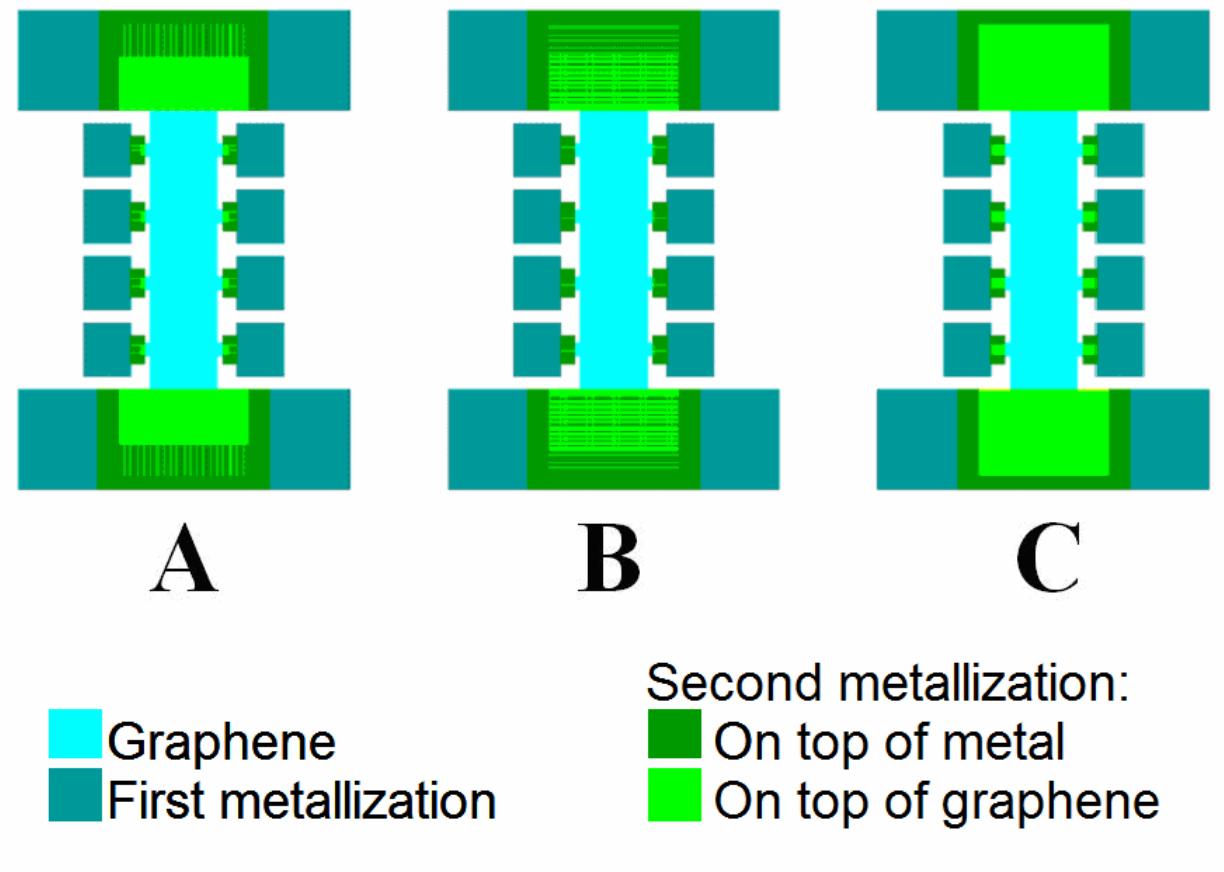

Figure 10. Patterning of the SiC samples that were used to study the influence of the type of contact for minimisation of contact resistance. Three different types of geometries were used, stripes in panel A, dot-like in panel B, and no additional patterning in panel C. All contacts were finally covered with gold.

Constant 10 μA current was applied trough the graphene devices and the voltage was measured by Keithley 236 Source-Measure Unit. Mobility and carrier concentration were estimated from the Hall resistance measurement. Results of the measurements and calculations are presented in Table 4. Annealing of the samples significantly reduced contact resistance for SiC121101 (for the contact of type A) and for SiC121010 (for the contact of type B), but for sample SiC121012 contact resistance is ten times higher (for both contacts types A and B) than the resistance of the not-annealed SiC121030. The lowest resistance from three tested types were those which use the stripe and dot-like contacts, panels A and B in Figure 10. A 5 nm graphite layer over graphene followed by the deposition of 5/50 nm of

Ti/Au during second metallization reduced the contact resistance in SiC121101 sample, device A, down 600 Ω. A similar device of type A in SiC121012 sample without additional graphite layer had contact resistance of 160 kΩ. It should be noted that this sample was dropped on the floor in a clean room during lithography, which also may be the reason of the increased contact resistance. To confirm the best possible type of contact, additional measurements with a larger number of samples should be done.

Table 4. Contact resistance of the SiC graphene samples with different types of contacts. Type A had striped contacts, type B dot-like contacts, and type C had no additional patterning of contact area (see Figure 10). The materials used in first metallization were titanium and gold for all four samples. The lowest resistance was obtained in sample SiC121101 with the contact of type A. This is possibly due to the layer of graphite under the Ti/Au used for covering the contacts. All samples in this table were made at the same time under the same growth temperature and time, with only difference in contact materials and annealing of the contacts after the lithography process.

Sample	**SiC121030**		**SiC121101**		**SiC121012**		**SiC121010**	
Annealing	**not annealed**		**annealed twice**		**annealed**		**annealed**	
Contacts (2^{nd} metallization)	**Ti/Au**		**C/Ti/Au**		**Ti/Au**		**Ti/Au**	
Device	**A2**	**B1**	**A2**	**C1**	**A1**	**B2**	**A1**	**B2**
Resistivity (μΩ·m)	49.20	44.50	3.57	3.23	56.12	28.78	8.09	12.35
Contact resistance (Ω)	17000	22000	600	1200	160200	170500	2800	900
Carrier concentration (10^{12} /cm^2)	1.25	0.89	1.25	1.25	2.08	0.89	3.47	1.64
Mobility (cm^2/Vs)	102	157	1200	1770	53	240	220	310

Different combinations of materials were used in contacts of CVD graphene samples in order to evaluate the reliability of contacts. Several contact materials were used together with gold: titanium, chromium, gold only, and graphite (on the second metallization) with titanium. In Table 5 the yield of the working and broken devices fabricated with different contacts is presented. Over the measurement period the most reliable contact type from the four tested

types was the one composed of titanium and gold contacts for the first metallization and graphite under titanium and gold for the second metallization. In addition to devices shown in Table 5, two CVD samples had a small alignment error in the lithography, and all devices from these samples were broken during the measurements. Samples were also used for quantum Hall measurements, which require cooling them down to temperatures of about 1.4 K, and many devices were broken during this temperature cycle. There may also have been some current spikes in the measurement devices that caused some contacts breaking. Some devices were broken after a long UV-irradiation. The SiC samples used in this study had no broken devices during the measurements. One sample was made with gold only contacts. All 15 devices of this sample were broken during measurements.

Table 5. Different types of the tested contacts and their reliability. Two samples with titanium contacts that had a small alignment problem are left out from this table. 100 % of those devices were broken, which shows that proper alignment is vital for reliability of the samples.

Contact type (1st metallization)	**Ti/Au**	**Au/Au**	**Ti/Au**	**Cr/Au**
Contact type (2nd metallization)	**Ti/Au**	**Au/Au**	**Graphite/Ti/Au**	**Cr/Au**
Devices	75	15	30	15
Broken devices	38	15	7	8
Broken, % of devices	51	100	23	53

3.5. Gas sensing measurements

3.5.1. Interaction of graphene with ozone

Preliminary measurement of the response of graphene sensors to high concentration of O_3 exposure was performed in MIKES by exposing samples to ozone and measuring the change in resistance. A 10 µA constant current from Keithley 2410 SourceMeter was applied trough the sample, and the voltage between two potential contacts on the side of the sample was measured by Agilent 3458A Digital Multimeter. Keithley 2000 Multimeter measured the resistance of the Pt100 sensor. Resistance of Pt100 resistor is proportional to temperature and was used to determine the temperature of the graphene sample. Ozone was produced from air flow of 20 l/h using Fischer 500M ozone generator. Results of ozone measurements are

presented in Figure 11. All samples showed decrease of resistance during ozone exposure. SiC sample was not as sensitive as CVD samples, so a higher level of concentration of O_3 was used for SiC samples. CVD samples were more sensitive, and they were able to sense small concentrations, at the level of 80 ppm. During the first 30 minutes of O_3 exposure, the resistance of CVD samples decreased by about 15 % - 23 %. Observed decrease of resistance showed that all tested samples are of p-type, because ozone is a p-type dopant [42]. Adsorbed O_3 molecules increase e-e scattering more on multi layer graphene than on single layer graphene [42], reducing mobility. This would suggest that epitaxial graphene sample SiC1312 has more graphene layers than the three CVD samples CVD120629, CVD120718#1 and CVD120718#2. CVD samples are specified by manufacturer (Graphene Labs inc.) to be monolayer with some double layer islands, and epitaxial samples are known to be often multilayer graphene [11,14,24].

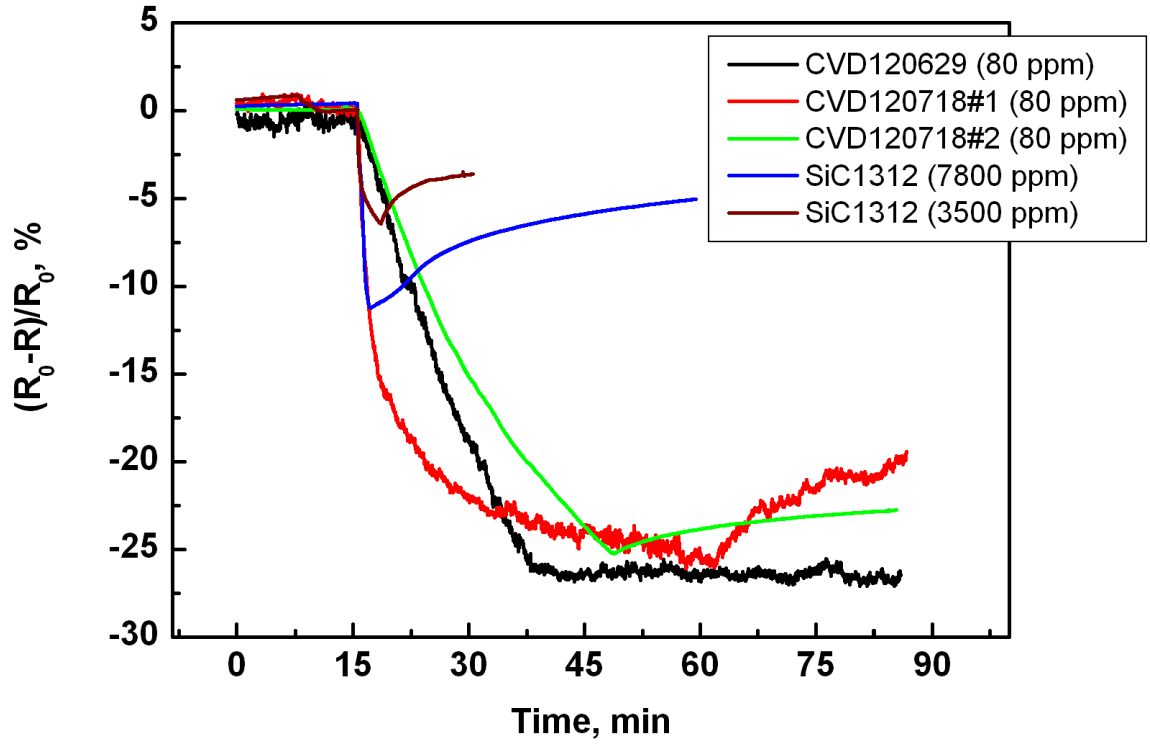

Figure 11. Change of resistance during exposure to ozone. Resistance of all samples decreases during ozone exposure, and starts to increase slowly once ozone generator is turned off. Ozone concentrations presented here (80 ppm - 7800 ppm) are only rough estimates. This measurement shows that ozone changes the resistance of graphene. SiC samples showed lower response to ozone, and they do not react on the smallest available concentrations.

For the measurement of the response of graphene to low concentrations of O_3 the CVD121003Gr sample was tested with a calibrated ozone source (Thermo Scientific Model 42i-TL) and Ozone meter (Enviromix Gas system Calibrator 6100) in Finnish Meteorological Institute. With the use of the calibrated ozone source, the samples were exposed to 20 ppb of O_3 which was enough to cause a change in resistance of CVD121003Gr sample by 0.4 %. Results from this measurement are presented in Figure 12. This measurement was done without the enclosure, in open air, as it was noticed previously that the brass enclosure adsorbs up to 40 % of ozone.

From Figure 12 it is seen that, unlike in Figure 11, the resistance increases when CVD121003Gr sample is exposed to ozone. That means that the sample has n type carriers and the carrier concentration is decreased when the sample is exposed to ozone gas which acts as electron acceptor.

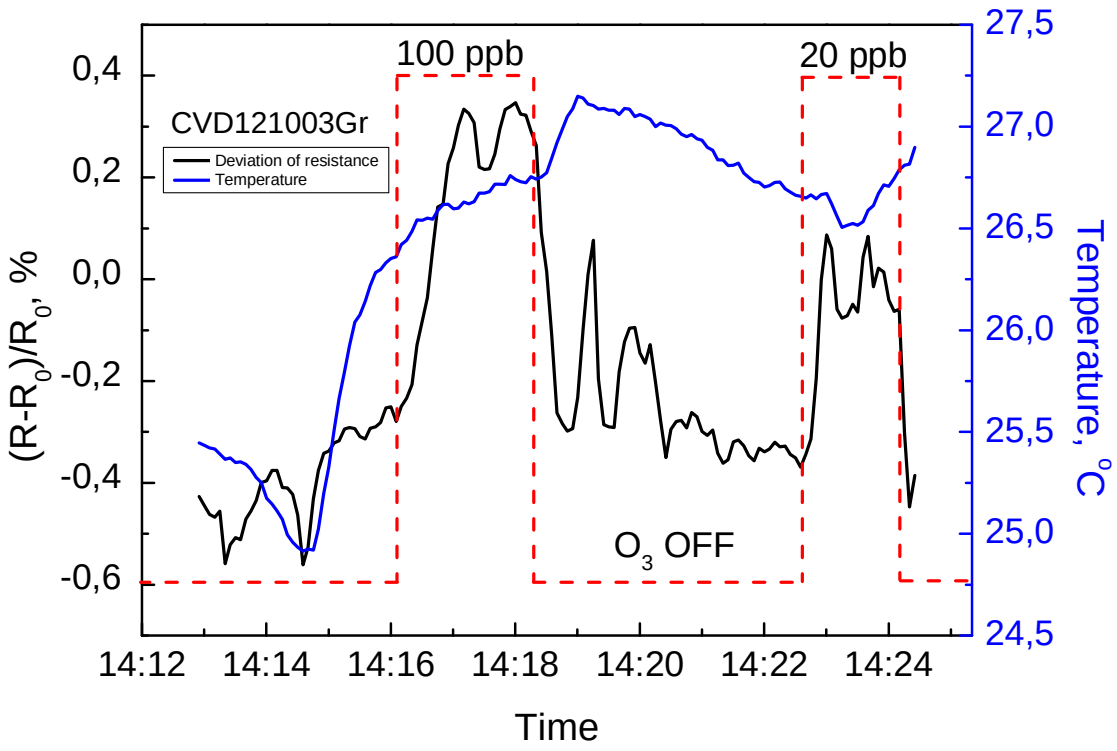

Figure 12. Measurement of sensitivity to ozone exposure in Finnish Meteorological Institute. CVD121003Gr shows response to even 20 ppb of O_3. Measurement is done in open air to prevent the influence of oxidation of brass enclosure.

3.5.2. Response of graphene samples to NO_2

Sensitivity of graphene to NO_2 was measured in Micronova, Aalto University. Constant current was applied trough graphene, and voltage was measured from potential contacts on the side of the device by Keithley 236 Source-Measure Unit, which was controlled by LabView software. NO_2 concentration in air flow was created by gas system presented in Figure 3. Keithley 2000 Multimeter was used to monitor temperature of the graphene sample.

To be used as reliable gas sensor, the response of graphene needs to have a systematic dependence on concentration of target gas. To determine the response, the graphene samples were exposed to different concentrations of NO_2 in different conditions. The measurement result of SiC120516 sample exposed for 10 minutes at 22 °C and 4 % relative humidity is presented in Figure 13. The results are summarized in Figure 14, which presents the resistive response of the sample versus NO_2 concentration. The response of SiC120516 sample

changed from increasing to decreasing resistivity during the measurement which indicates inversion of the carrier type. Other two samples, CVD121003Gr, SiC121003 showed decreasing resistance to all concentrations measured at room temperature. The resistance change presented in Figure 14 is calculated as the difference of resistance between the time when NO_2 flow is turned on and the time when it is turned off. The magnitude of the change depends on recovery time between exposures. Recovering from NO_2 exposure can take several hours, even days, if the samples are not cleaned, for example, by heating. The change in resistance during NO_2 exposure is not reproducible and does not have a systematic dependence on NO_2 concentration at room temperature. Thus the tested samples are not very useful NO_2 sensors at room temperature

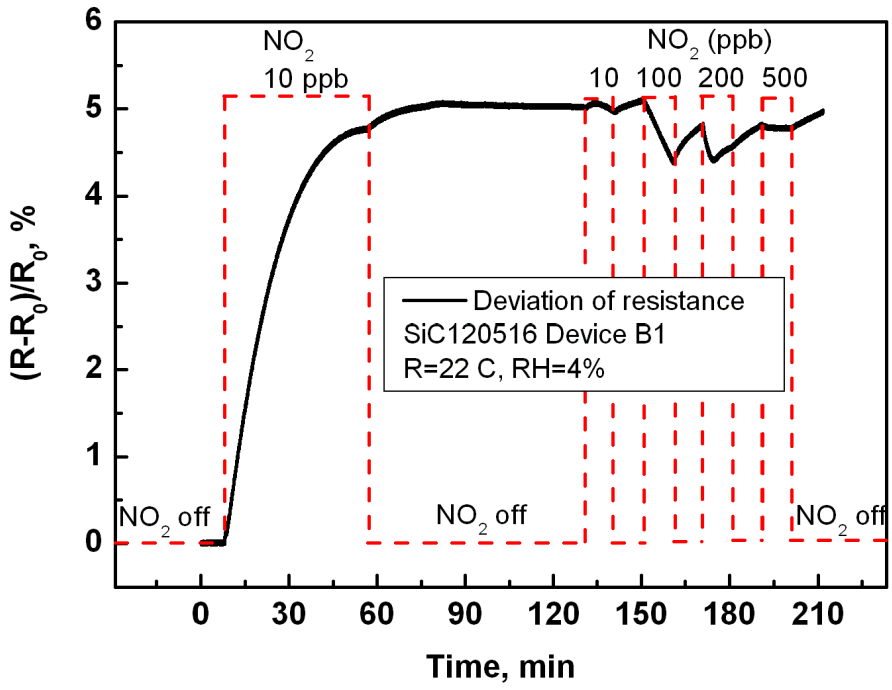

Figure 13. Results of the response measurement of SiC120516 sample. First, the sample was exposed to 10 ppb of NO_2 for 30 min. After recovery from the first exposure, the sample was exposed to 10 ppb of NO_2 during 10 minutes, followed by 10 minute of recovery, then the sample was exposed to 100 ppb, to 200 ppb and to 500 ppb concentrations of NO_2. Direction of response was changed during measurement from increasing of resistance (at first 30 minute of exposure to 10 ppb of NO_2), to decreasing, during the first 10 minute of exposure to 10 ppb, and then back to increasing resistance at 200 ppb. During exposure of the sample to 500 ppb the resistance decreases, but only slightly, less than 0.1 %. Measurements were performed in flow of carrier gas of 1100 cm^3/min, at temperature 22 °C and relative humidity 4 %.

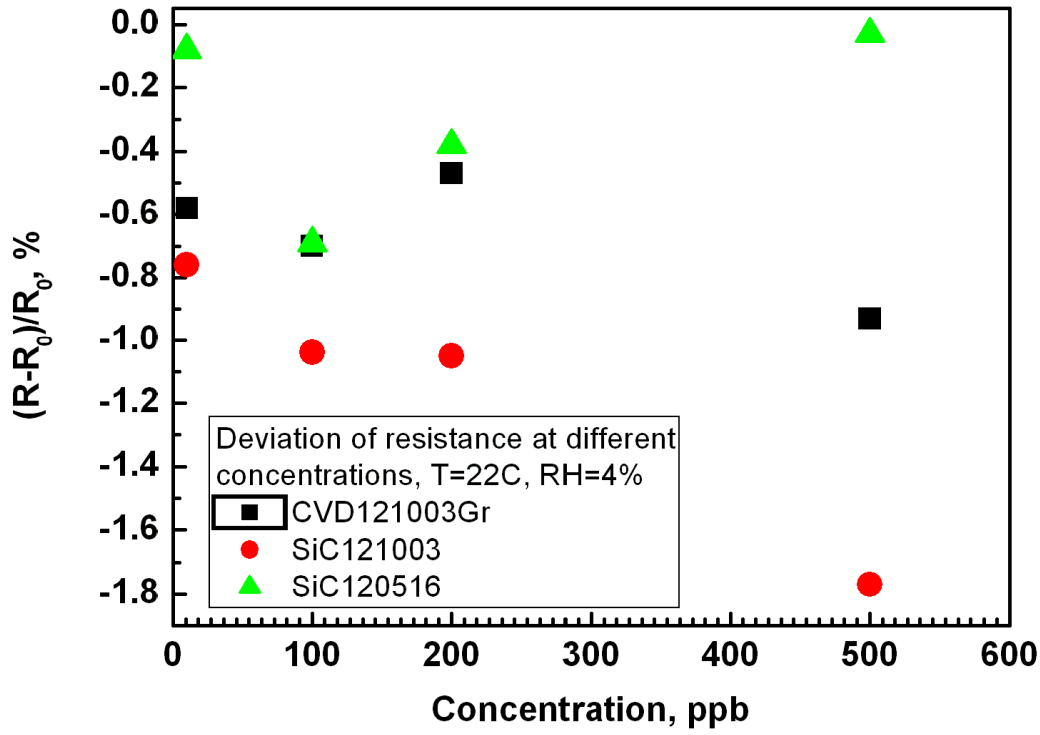

Figure 14. Deviation of resistance in three different graphene samples during 30 minutes of exposure to different concentrations of NO_2 at room temperature. Response is not predictable and depends on the history of the device

The situation improves clearly when the samples are heated to an elevated temperature. In Figure 15, results of exposure to different concentrations of NO_2 during 200 seconds at temperatures above 100 °C for the sample SiC121003 are presented. Exposure to 10 ppb is repeated 4 times to show repeatability of the response. Results of the resistive responses of SiC121003, SiC120516 and CVD121003 samples versus applied NO_2 concentration are summarized and presented in Figure 16. The linearity and reproducibility of the response was improved by heating and the magnitude of response was increased in the three tested samples. SiC120516 sample shows the increase in resistance, which would indicate n-type charge carriers, because NO_2 is an acceptor of electrons, and reducing carrier concentration would increase the resistance of the graphene. Two other samples, SiC121003 and CVD121003Gr show decreasing resistance, indicating increased number of charge carriers, and p-type conductivity.

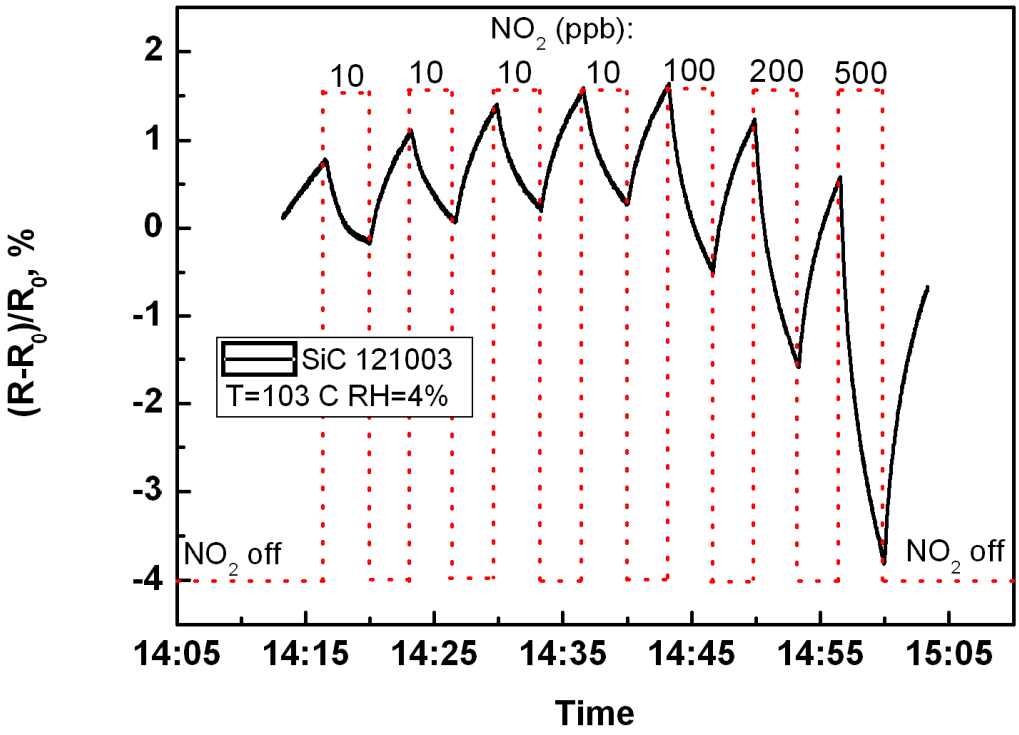

Figure 15. SiC121003 sample was exposed to NO_2 for 200 seconds, followed by 200 seconds recovery, first four times with 10 ppb then once with 100 ppb, 200 ppb and 500 ppb concentrations. Resistance of SiC121003 decreased during the exposure to NO_2. Measurement was performed in flow of 1100 cm^3/min, at temperature 103 °C and relative humidity 4 %.

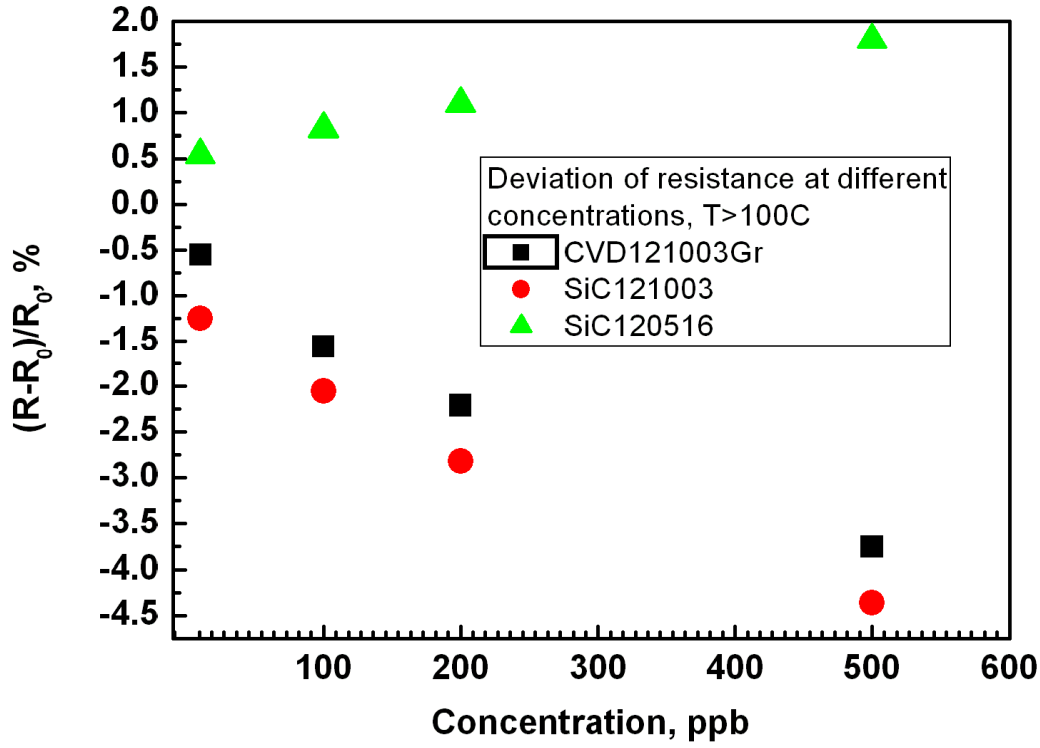

Figure 16. Deviation of resistance in three graphene samples during 200 second exposure to different concentrations of NO_2 in temperatures above 100 °C. Change in resistance increases for SiC120516 sample with increasing concentration, while SiC121003 and CVD121003Gr samples show decrease of resistance.

The samples were tested for their response to exposure on 10 ppb of NO_2 during 200 s in relative humidity around 70 % and temperature 22 °C. Results of measurement performed with SiC121003 sample are presented in Figure 17. In this figure a delay in response is clearly seen. This delay may be due to something in the gas system used that delays the NO_2 reaching the enclosure. Another possibility is that NO_2 reacts with water in the gas flow to form acid and this delays the NO_2 reaching the graphene sample. Results of resistance change versus NO_2 concentration obtained from similar measurements with SiC120516, SiC121003 and CVD121003 samples are summarized and presented in Figure 18. In high humidity, the response to exposure and switching of NO_2 ON and OFF was delayed for about one minute for all samples. The response for SiC121003 sample at high humidity level is increased from the response measured at low humidity at room temperature, but reduced for CVD121003Gr. The change in resistance under high humidity conditions in SiC120516 sample did not have a systematic dependence on NO_2 concentration. For SiC121003 and CVD121003Gr samples resistive response to NO_2 exposure in high humidity and room temperature was more

systematic compared to low humidity exposure in room temperature. This may be because the magnitude of response is also increased which hides the effect of the random impurities before the exposure on the graphene plane. Water molecules act as electron donors, they increase resistance of the p-type graphene as is seen from Figure 17. The increase of resistance in the beginning of measurement was during the humidity increase. From the decrease of resistance during NO_2 exposure we can say that graphene sample SiC121003 is of p-type. When a water molecule on graphene surface is replaced by NO_2 molecule, the decrease of resistance is bigger than when NO_2 molecule is adsorbed on empty graphene surface, because the desorbed water molecule and adsorbed NO_2 molecule both increase the carrier (hole) concentration.

As the humidity in ambient air is often very high the graphene devices need to be working in high humidity conditions. One way to possibly provide operation of the graphene in high humidity is to find the optimal working temperature. This may help get rid of residual gasses and impurities on graphene before measurement, and yield more reliable measurements of gas concentration.

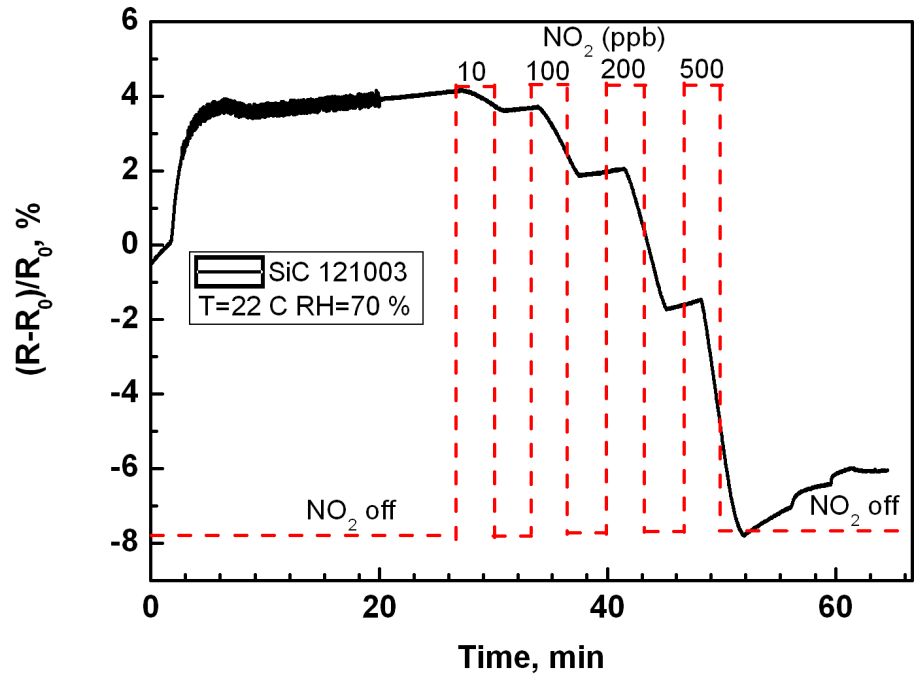

Figure 17. Deviation of resistance under high humidity conditions in SiC121003 sample. A delay between turning the NO_2 flow on and beginning of a change in the resistance was about one minute. Similar delay was noticed when turning the NO_2 off. Initial rise in resistance is due to increasing humidity from 4 % RH to 70 % RH.

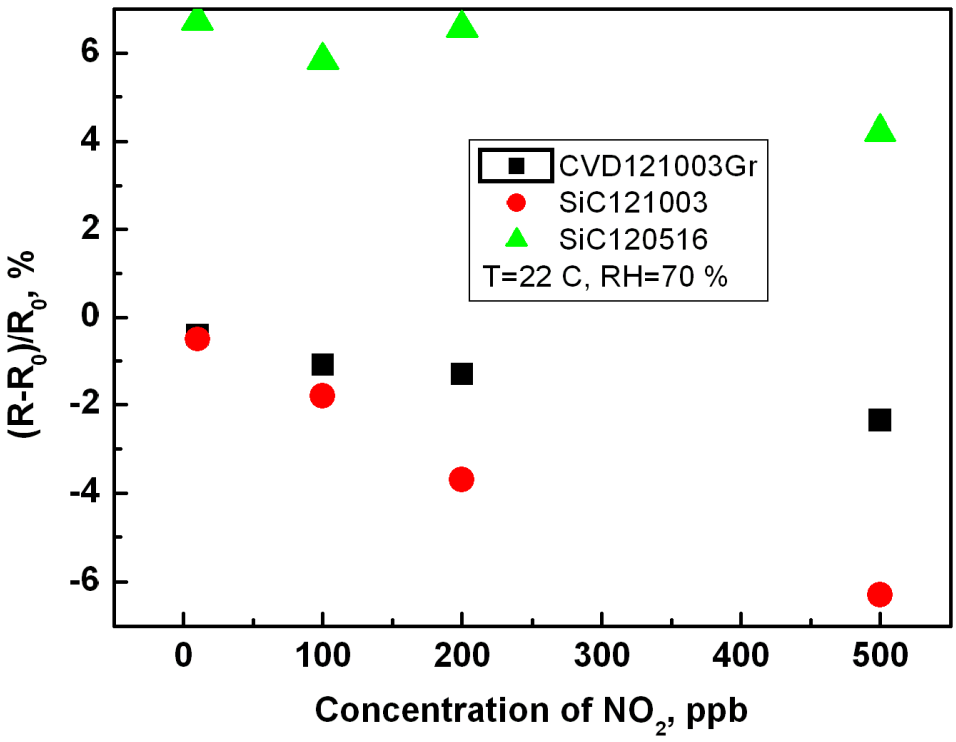

Figure 18. Deviation of the resistance during exposure to NO_2 for 200 s at room temperature in high humidity, as a function of NO_2 concentration. 70 % relative humidity was achieved by directing all carrier gas trough water. Response to exposure for both samples, SiC121003 and CVD121003Gr is delayed in high humidity: the change in resistance starts about one minute after NO_2 flow is turned on or off. This delay is taken into account here by calculating the deviation from the time when the resistance starts to decrease (increase for SiC120516), until the time when the resistance starts to increase again (decrease for SiC120516).

Temperature dependence of the response to 10 ppb of NO_2 for 200 s between 22 °C and 45 °C, at relative humidity of 4 % was tested for SiC121003 sample. Measurements below 25 °C were performed under UV-irradiation and at 70 % relative humidity too. The results of this measurement are presented in Figure 19. A change in direction of the response was noticed above 40 °C. This is possibly due to the change in carrier type above 40 °C, from n-type to p-type. The resistance decreased when relative humidity was increased from 4 % to 70 % (opposite to Figure 17), and response to NO_2 was stronger under high humidity. UV-light increased response only slightly in low humidity, but when relative humidity was 70 %, UV-light decreased sensitivity.

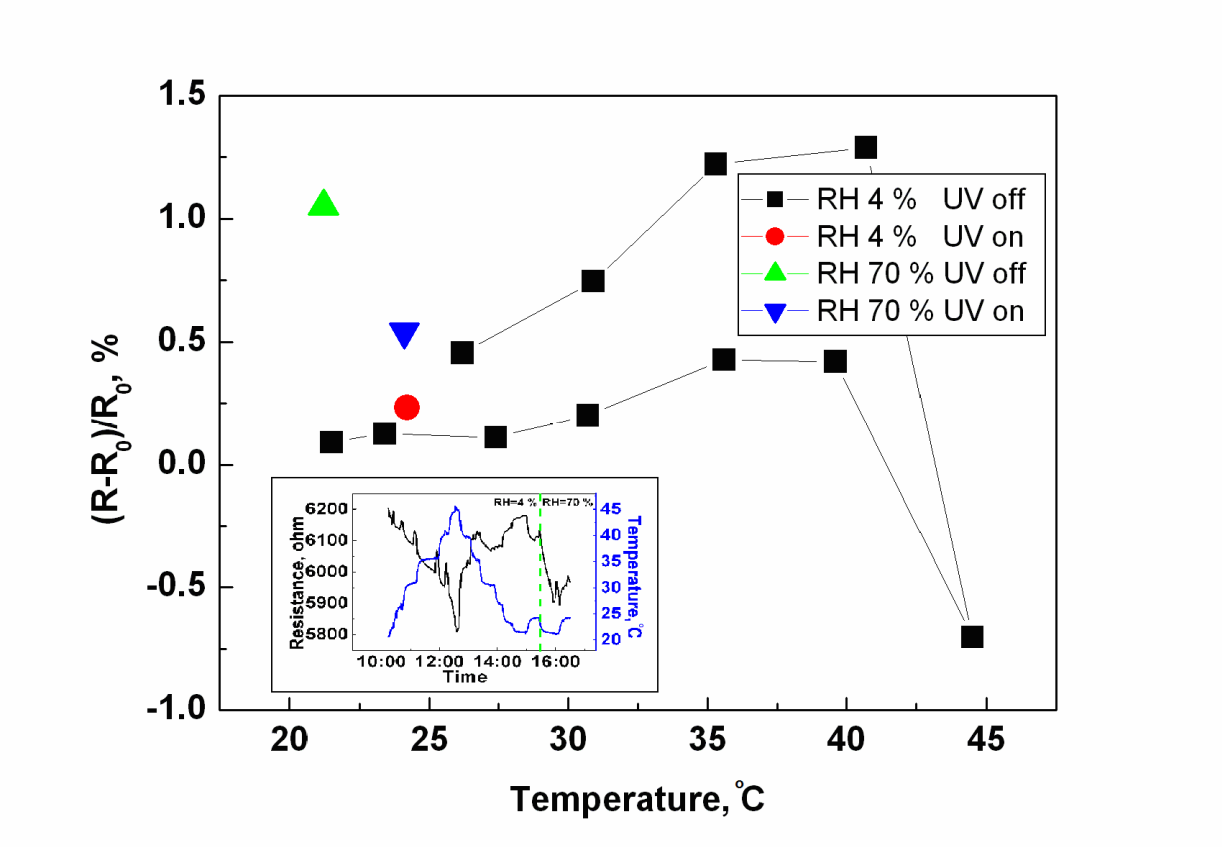

Figure 19. Change in resistance during 200 s exposure to 10 ppb of NO_2 for SiC121003 at different temperatures. Black squares represent results of NO_2 exposure in 4 % relative humidity without UV-light. Red circle presents result of NO_2 exposure under UV-light in 4 % humidity at 24 °C, green triangle presents the result of NO_2 exposure without UV-light in 70 % humidity at 22 °C, and blue triangle presents result of NO_2 exposure under UV-light in 70 % humidity and at 24 °C. The resistive response to exposure is positive and increases with temperature, until above 40 °C, where the sign of response is changed. In the inset the resistance of SiC121003 and the temperature during the same measurement are presented. The resistance of the sample decreases with temperature and a decrease is noticed when relative humidity is increased from 4 % to 70 % (green vertical line in inset).

In the experiments of Figure 19, the influence of the heating on adsorption and desorption rates of the NO_2 gas were studied by exposing graphene samples to 10 ppb of NO_2 for a short period of time (200 s). To perform more reliable measurement of the influence of temperature, longer time would be needed between exposures, so that the sample would recover fully and all NO_2 molecules from the last exposure would be desorbed from the graphene surface. To speed up the recovery, desorption time of the gas molecules should be decreased. The shorter time it takes for molecules to desorb, the faster the surface is cleaned from residual NO_2 molecules, and the faster the sensor can be reused. Desorption time of molecules may be decreased by heating or UV-irradiation.

Another way to investigate the effect of temperature and other parameters on the response of the sensors is to measure the initial rate of resistance change when the gas exposure is switched on or off. The initial response and recovery rates were evaluated as deviation of resistance (in %) during the first five seconds of exposure and recovery, divided by five seconds, to estimate time derivative of the initial change of resistance. Five second period was used because it was short enough to estimate derivatives but long enough to eliminate effects of noise. Measurements were done on four epitaxial graphene samples, SiC121010, SiC121012, SiC121030, and SiC121101, used in contact resistance measurements earlier. Three devices of each sample were measured at the same time, except for SiC121012, in which only two devices were bonded. The contact type, the carrier concentration and mobility of these samples are shown in Table 4.

To measure several devices simultaneously, two different measurement units were used. Keithley K236 was used to measure one device, and a measurement/source unit made in MIKES was used to measure the other two devices. The unit which was made in MIKES had two current sources and two measurement inputs, which could be used as two separate source/measure units, or as two voltage measurement channels and one current source. In these measurements all devices were measured separately. Because of the limited number of connecting pins, each device was measured by two terminal measurement, which does not eliminate the resistance of leads and contacts.

To compare four SiC samples, the time derivative of the response at different temperatures was measured with the same concentration of NO_2, 10 ppb, and the results are presented in Figure 20. The SiC121010 sample (presented in Figure 20 (b)) has the largest derivative, i.e. the optimal operating temperature, around 100 °C, and for SiC121030 (presented in Figure 20 (c)) the optimum temperature is around 80 °C. For SiC121101 (presented in Figure 20 (a)) and SiC121012 (presented in Figure 20 (d)) the derivative is still increasing above 100 °C, so the optimal temperature is higher than that of SiC121010 and SiC121030.

The influence of temperature is most systematic in twice annealed sample with graphite layer under Ti/Au used in covering the contacts (second metallization), SiC121101. The magnitude of the derivative for SiC121101 sample is large, up to 3 % / s. This sample also has the highest mobility 1200 cm^2 / Vs. SiC121010 has the highest carrier concentration and the highest derivative of the response, up to 5.5 % / s in room temperature (22 °C), and about 7 % / s at 100 °C. There was no difference in fabrication of SiC121012 and SiC121010, but SiC121012 had significantly lower derivative of response (< 1 % / s at all measured

temperatures). SiC121012 was dropped on the floor during lithography, which may have influenced its electric properties.

The influence of temperature on the rate of recovery is presented in Figure 21. The recovery rate increases with increasing temperature for all samples. The temperature response is most systematic in twice annealed sample with graphite layer under Ti/Au used in covering the contacts (second metallization), SiC121101 (see Figure 21 (a)). Largest recovery rates were in SiC121101 and SiC121010 (see Figure 21 (b)) samples, of about - 0.9 % / s at 100 °C. SiC121030 (see Figure 21 (c)) had recovery rate of about -0.4 % / s, and SiC121012 (see Figure 21 (d)) of about -0.6 % / s at 120 °C. Adding a graphite layer during the second metallization may reduce the effect of contact resistances on response and reduce the dependence on the contact area (contact types A, B and C in Figure 10) on sample SiC121101. All other samples have big difference between different contact types. Annealing the sample increased the derivative for sample SiC121010, compared to not annealed sample (with same Ti/Au contacts) SiC121030.

When the graphene devices recover from the exposure to NO_2, no adsorption of molecules should take place. Thus the recovery rate must depend on the desorption rate only. The recovery rate increases for all samples with increasing temperature. The desorption rate of molecules from graphene surface can thus be increased by increasing temperature. This effect can be used to clean graphene samples after exposure. Response to the exposure depends on both the rate of molecules being adsorbed on the graphene surface (adsorption rate), and desorption of molecules from the graphene surface (desorption rate). Response rate increases in all samples with increasing temperature, until certain temperature. This means that the adsorption rate increases faster than the desorption rate with increasing temperature until a certain temperature.

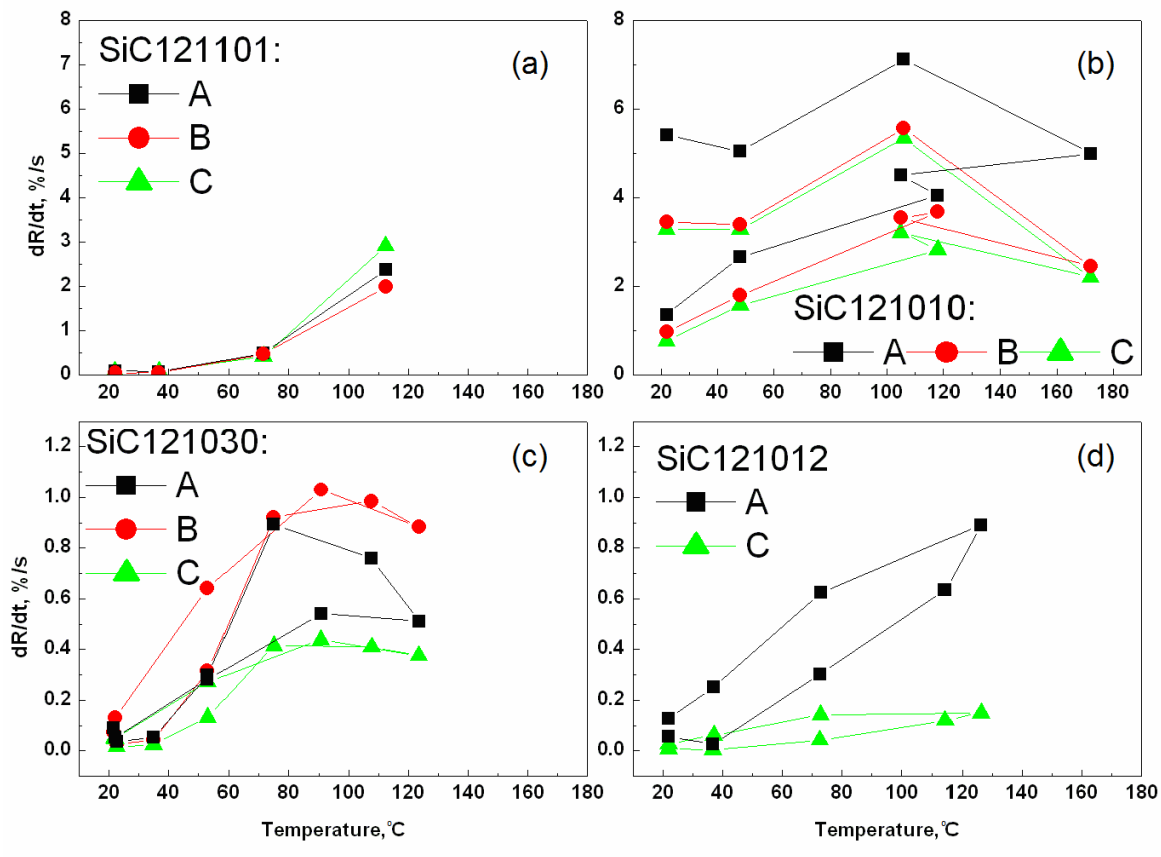

Figure 20. Initial rate of resistive response to 10 ppb of NO_2 at different temperatures for (a) SiC121101 sample, (b) SiC121010 sample, (c) SiC121030 sample, and (d) SiC121012 sample. Resistance of all samples increases during exposure to NO_2 gas. Results are presented as the derivative of the relative change of resistance. A, B, and C refer to the devices with different types of contacts, which are explained in section 3.4 and presented in Figure 10.

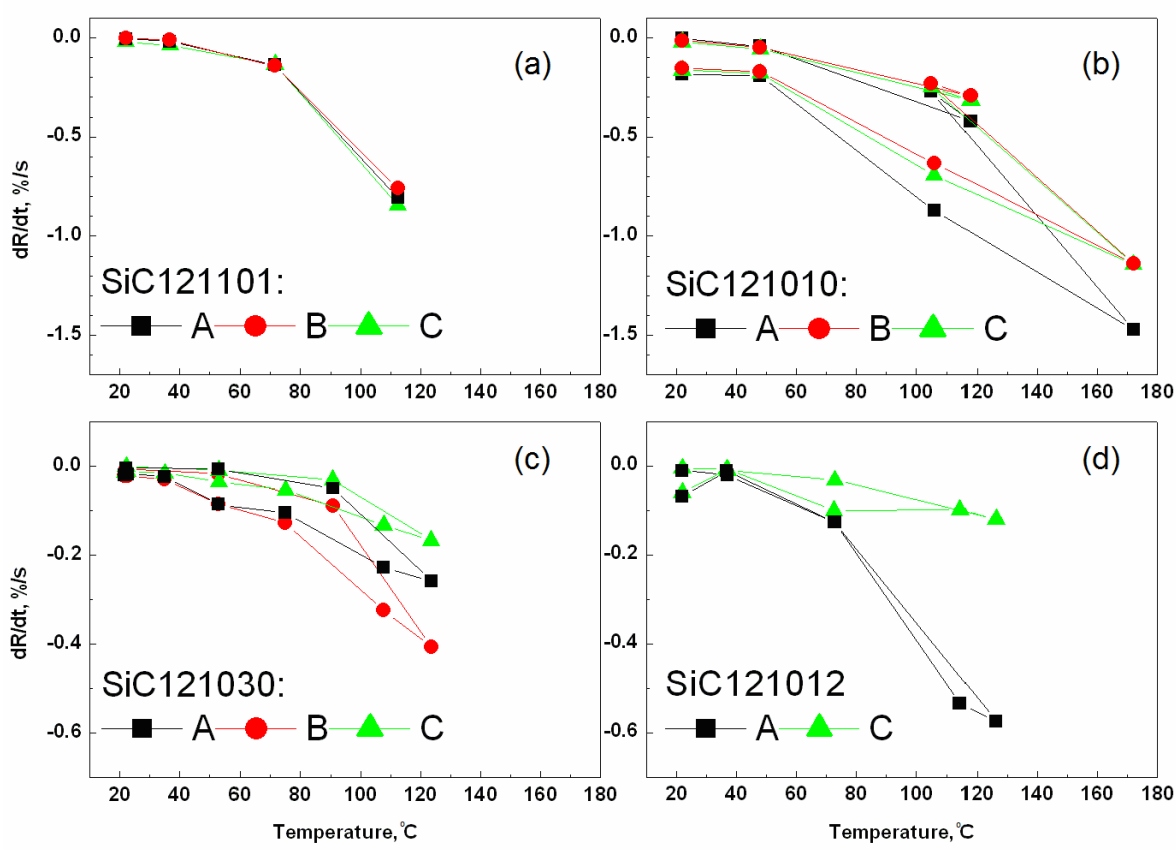

Figure 21. Time derivative of the recovery after application of 10 ppb of NO_2 at different temperatures exposed during 200 seconds for (a) SiC121101 sample, (b) SiC121010 sample, (c) SiC121030 sample, and (d) SiC121012 sample. The magnitude of derivative increases with increasing temperature. Devices A, B, and C refer to the devices presented in section 3.4 and shown in Figure 10.

4. Conclusions

Several CVD and epitaxial SiC samples were investigated to find the optimal conditions for gas sensing applications. UV-irradiation, different temperatures and relative humidities were used to find the biggest response and most predictable behaviour as a function of gas concentration.

The effect of UV-irradiation on the resistance of graphene samples was studied to achieve low carrier concentration and high mobility, which are preferred in gas sensor applications. Samples were irradiated with 370 nm wavelength UV-LED for 30 minutes. The tested CVD samples had higher sensitivity to UV light, about 60 % -110 % increase in resistance during the irradiation, while the resistance of the SiC samples increased less, by 8 % -15 %.

The effects of UV-irradiation and temperature on the carrier concentration and mobility of SiC and CVD samples were evaluated using the measurement of the Hall resistance in low (0.1 T) magnetic field just before and immediately after UV-irradiation and heating. The carrier concentration was decreased from 12 $\cdot 10^{11}$ /cm^2 to 5 $\cdot 10^{11}$ /cm^2 and the mobility was increased from 2000 cm^2/Vs to 4500 cm^2/Vs by heating CVD121009Eu sample from room temperature up to 50 °C. UV-irradiation also increased the mobility and decreased the carrier concentration in all three tested CVD samples: CVD121009Eu, CVD120718#1, and CVD120802Ti. UV illumination had the strongest influence on CVD121109Eu sample, whose mobility increased from 3000 cm^2/Vs to 4000 cm^2/Vs, and the carrier concentration decreased from $11 \cdot 10^{11}$ /cm^2 to $6 \cdot 10^{11}$ /cm^2.

Different types of contacts were tested for improving stability and reducing contact resistance. From the four tested combinations, gold only, titanium under gold, chromium under gold, and graphite under titanium and gold, the graphitic contacts were most reliable during the measurement period, whereas the gold only contacts were the most unreliable ones. More research is needed to ensure reliability of the contacts and to find the best possible combination of materials. Three different geometries of contacts were also tested. The smallest resistance was obtained with striped contacts, while the highest contact resistance was obtained without additional patterning between graphene and contact metal. Annealing normally decreased contact resistance, but one of the annealed samples had very high contact resistance, around 150 kΩ. Adding a graphite layer under metal during the second metallization reduced contact resistances. The smallest achieved contact resistance was about 600 Ω.

Graphene SiC and CVD samples were tested for their ability to sense O_3 gas in air flow (20% O_2 and 80% N_2). All tested samples showed decrease in resistance when exposed to O_3. Epitaxial SiC graphene samples did not sense the lowest available O_3 concentration of about 80 ppm, so a higher concentration (5000 ppm) was used for them. The resistance of three CVD samples decreased by 15 % -23 % during the first 30 minutes of exposure with 80 ppm O_3 concentration. These results give confidence that graphene thin film samples can be used to sense ozone. In the measurement of response to ozone performed in Finnish Meteorological Institute, a clear response to 20 ppb of O_3 was observed. This study shows that graphene can be used as highly sensitive sensor for small concentrations of O_3. Ozone has been known to cause the changes in conductivity of graphene and has been used to improve graphene's ability to sense other gasses, but no study has been previously published about use of CVD or epitaxial graphene as an ozone detector.

The main goal of this study was to improve the sensitivity of graphene samples to NO_2 gas. The minimum concentration available, 10 ppb of NO_2, could be detected by SiC and CVD based graphene devices. Increase in sensitivity and more predictable behaviour was obtained by heating the samples. Optimal temperature of graphene for gas sensing applications depends on the sample. High humidity decreased sensitivity of CVD sample (CVD121003Gr), while the sensitivity of two tested SiC samples increased in high humidity conditions. For real life applications performance in high humidity conditions is vital, because outside air may have even higher relative humidity than was available in this study. Even though detection of sub-ppb-level of concentration of NO_2 gas by CVD pristine graphene has been reported recently [23], and even individual NO_2 molecules have been detected by exfoliated graphene sensors [15], development of graphene sensors for sub-ppm level detection of NO_2 is still an international challenge. Before this work, sensitivity of SiC graphene to 10 ppb concentration of NO_2 gas in air has been reported only by the MIKES-Aalto collaboration [24].

The measurements of temperature dependence of the response to NO_2 gas showed that the adsorption and desorption rates to/from the graphene surface increase with temperature, and the heating can be used to clean the samples after exposure. The sensitivity to NO_2 increased with temperature, up to a certain temperature (depending on the sample), which suggests that adsorption of the NO_2 molecules on graphene surface increases with increasing temperature, but after the optimal temperature, the desorption starts to dominate and sensitivity of the devices decreases.

5. References:

1. S. Capone, A. Forleo, L. Francioso, R. Rella, P. Siciliano, J. Spadavecchia, D. S. Presicce and A. M. Taurino: *Solid State Gas Sensors: State of the Art and Future Activities,* Journal of Optoelectronics and Advanced Materials **5,** 1335–1348 (2003)
2. P. Krebs and A. Grisel: *A low power integratedatalytic gas sensor,* Sensors and Actuators B: Chemical **13,** 155–158 (1993)
3. A.K. Geim and K.S. Novoselov: *The Rise of Graphene,* Nature Materials **6**, 183–191 (2007)
4. E.J. Duplock, M. Scheffler and P.J.D. Lindan: *Hallmark of Perfect Graphene,* Physical Review Letter **92**, 225502 (2004)
5. S.Y. Zhou, G.-H. Gweon, A.V. Fedorov, P.N. First, W.A. de Heer, D.-H. Lee, F. Guinea, A.H. Castro Neto and A. Lanzara: *Substrate-induced band gap opening in epitaxial graphene,* Nature Materials **6**, 770–775 (2007)
6. D.Gunlycke, H.M. Lawler and C.T.White: *Room temperature ballistic transport in narrow graphene strips,* Physical review B **75,** 085418 (2007)
7. S.Y. Zhou, G.-H. Gweon, J. Graf, A.V. Fedorov, C.D. Spataru, R.D. Diehl, Y. Kopelevich, D.-H. Lee, S. G. Louie and A. Lanzara: *First direct observation of Dirac fermions in graphite,* Nature Physics **2,** 595–599 (2006).
8. C. Soldano, A. Mahmood and E. Dujardin: *Production, properties and potential of graphene,* Carbon **48,** 2127–2150 (2010)
9. J. Hass, W. A. de Heer and E. H. Conrad: *The growth and morphology of epitaxial multilayer graphene,* J. Phys. Condens. Matter **20,** 323202 (2008).
10. F. Varchon, R. Feng, J. Hass, X. Li, B. Ngoc Nguyen, C. Naud, P. Mallet, J.-Y. Veuillen, C. Berger, E. H. Conrad and L. Magaud: *Electronic Structure of Epitaxial Graphene Layers on SiC: Effect of the Substrate,* Physical Review Letters **99**, 126805 (2007)
11. W.A. de Heer, C. Berger, X. Wu, P. N. First, E.H. Conrad, X. Li, T. Li, M. Sprinkle, J. Hass, M.L. Sadowski, M. Potemski, G. Martinez: *Epitaxial graphene,* Solid State Communications, **143**, 92–100 (2007)
12. A. Grüneis, K. Kummer and D. V. Vyalikh: *Dynamics of graphene growth on a metal surface: a time-dependent photoemission study,* New Journal of Physics **11,** 073050 (2009).
13. M. Borysiak*: Graphene synthesis by CVD on copper substrates,* NNIN REU Research accomplishments, 70–71 (2009).

14. B.K. Daas, W.K.Nomani, K.M.Daniels, T.S. Sudarshan, Goutam Koley and M.V.S. Chandrashekhar: *Molecular Gas Adsorption Induced Carrier Transport Studies of Epitaxial Graphene using IR Reflection Spectroscopy,* Materials Science Forum **717 – 720**, 665-668 (2011)
15. F. Schedin, A. K. Geim, S. V. Morozov, E. W. Hill, P. Blake, M. I. Katsnelson and K. S. Novoselov: *Detection of individual gas molecules adsorbed on graphene,* Nature materials **6**, 652 - 655 (2007).
16. O. Leenaerts, B.Partoens and F.M. Peeters: *Adsorption of H_2O, CO, NO_2, and NO on graphene: A first-principles study,* Physical Review B **77**, 125416 (2008)
17. J. Yan, Y. Zhang, P. Kim and A. Pinczuk: *Electric Field Effect Tuning of Electron-Phonon Coupling in Graphene,* Physical Review Letters **98**, 166802 (2007)
18. S.Y. Zhou, D.A. Siegel, A.V. Fedorov and A. Lanzara: *Metal to insulator transition in epitaxial graphene induced by molecular doping,* Physical review letters **101**, 086402 (2008)
19. G.U. Sumanasekera, G. Chen, K. Takai, J. Joly, N. Kobayashi, T. Enoki and P.C. Eklund: *Charge transfer and weak chemisorption of oxygen molecules in nanoporous carbon consisting of a disordered network of nanographene sheets,* Journal of Physics: Condensed Matter **22,** 334208 (2010)
20. J. Fowler, M. Allen, V. Tung, Y. Yang, R. Kaner and B. Weiller: *Practical Chemical Sensors from Chemically Derived Graphene,* ACS Nano **3,** 301-306 (2009)
21. H. J. Yoon, D. H. Jun, J. H. Yang, Z. Zhou, S. S. Yang and M. M.-C. Cheng: *Carbon dioxide gas sensor using a graphene sheet,* Sensors and Actuators B: Chemical **157,** 310-313 (2011)
22. F. Yavari, E. Castillo, H. Gullapalli, P.M. Ajayan and N. Koratkar: *High sensitivity detection of NO_2 and NH_3 in air using chemical vapor deposition grown graphene,* Applied Physics Letters **100**, 203120 - 203120-4 (2012)
23. G. Chen, T.M. Paronyan and A.R. Harutyunyan: *Sub-ppt gas detection with pristine graphene,* Applied Physics Letters **101**, 053119 (2012)
24. S. Novikov, A.Satrapinski, N. Lebedeva and I. Iisakka: *Sensitivity optimization of epitaxial graphene based gas sensors,* IEEE Transactions on Instrumentation and Measurement **99**, in press (2013)
25. H. Y. Jeong, D.-S. Lee, H. K. Choi, D. H. Lee, J.-E. Kim, .J. Y. Lee, W. J. Lee, S. O. Kim and S.-Y. Choi: *Flexible room-temperature NO_2 gas sensors based on carbon nanotubes/reduced graphene hybrid films,* Applied Physics Letters **96**, 213105 (2010)

26. Y. C. Cheng, T. P. Kaloni, Z. Y. Zhu, and U. Schwingenschlögl: *Oxidation of graphene in ozone under ultraviolet light*, Applied Physics Letters **101**, 073110 (2012)
27. N. Leconte, J. Moser, P. Ordejón, H. Tao, A. Lherbier, A. Bachtold, F. Alsina, C.M. Sotomayor Torres, J.-C. Charlier and S. Roche: *Damaging Graphene with Ozone Treatment: A Chemically Tunable Metal−Insulator Transition*, ACS Nano **4**, 4033–4038 (2010)
28. E.X. Zhang, A.K.M. Newaz, B. Wang, C.X. Zhang, D.M. Fleetwood, K.I. Bolotin, R.D. Schrimpf, S.T. Pantelides and M.L. Alles: *Ozone-exposure and annealing effects on graphene-on-SiO_2 transistors*, Applied Physics Letters **101**, 121601 (2012)
29. L. Lozz, S. Santucci, C. Cantalini, C. Baratto, G. Sberveglieri, I. Armentano, J.M. Kenny, L. Valenti and B. Delley: *Ozone reactivity with carbon nanotubes: experimental and theoretical studies*, Proceedings of IEEE, 436-439 (2003)
30. G. Chen and A. R. Harutyunyan: *Method of enhanced detection for nanomaterial-based molecular sensors*, U.S. patent 20120282594 A1 (2012)
31. K. Nagashio and A. Toriumi: *Density-of-States Limited Contact Resistance in Graphene Field-Effect Transistors*, Japanese Journal of Applied Physics **50,** 070108 (2011)
32. C. Gong, G. Lee, B. Shan, E.M. Vogel, R.M. Wallace and K. Cho: *First-principles study of metal–graphene interfaces*, Journal of Applied Physics **108**, 123711 (2010)
33. Y. Matsuda, W.-Q. Deng and W. A. Goddard: *Contact Resistance for "End-Contacted" Metal-Graphene and Metal-Nanotube Interfaces from Quantum Mechanics*, Journal of Physical Chemistry C **114**, 17845–17850 (2010)
34. H. Ibach and H. Lüth: *Solid State Physic - An introduction to Principles of Materials Science 2nd edition*, Springer (1995)
35. J.R. Taylor: *Error Analysis, the Study of Uncertainties in Physical Measurements, 2nd edition*, University science books (1997)
36. H.D. Young and R.A Freedman: *University Physics with Modern Physics 12th Edition*, Pearson (2007)
37. H. Juretić, S. Dobrović, N. Ružinski, J. Lovrić, M. Pećarević, J. Mikuš, M. Crnčević, E. J. Marčelja, M. M. Rajčić and W. J. Cooper: *Pilot study on ozonation as a possible treatment for ballast water*, UNESCO UCI Groundwater Conference Proceedings (2008)
38. Z. Luo, N.J. Pinto, Y. Davila and A.T.C. Johnson: *Controlled doping of graphene using ultraviolet irradiation*, Applied Physics Letters **100**, 253108 (2012)
39. J. Moser, H. Tao, S. Roche, F. Alzina, C. M. Sotomayor Torres and A. Bachtold: *Magnetotransport in disordered graphene exposed to ozone: From weak to strong localization*, Physical review B **81**, 205445 (2010)

40. J. Malicet, D. Daumont, J. Chabonnier, C. Parisse, A. Chakir and J. Brion: *Ozone UV Spectroscopy. II. Absorption Cross-Sections and Temperature Dependence*, Journal of Atmospheric Chemistry **21,** 263-273 (1995)
41. S. Novikov, J. Hämäläinen, J. Walden, I. Iisakka, N. Lebedeva and A. Satrapinski, *Characterisation of epitaxial and CVD graphene with double metal-graphene contacts for gas sensing*, Abstract acccepted for the 16th International Congress of Metrology, October 7-10, 2013, Paris
42. F. Alzina, H. Tao, J. Moser, Y. Garcia, A. Bachtold and C. M. Sotomayor-Torres: *Probing the electron-phonon coupling in ozone-doped graphene by Raman spectroscopy*, Physical Review B **82,** 075422 (2010)